Gondwana Research 93 (2021) 275–290

Contents lists available at ScienceDirect

Gondwana Research

journal homepage: www.elsevier.com/locate/gr

Tectonically-induced strontium isotope changes in ancient restricted seas: The case of the Ediacaran-Cambrian Bambuí foreland basin system, east Brazil

Cristian Guacaneme [a,*], Marly Babinski [a], Carolina Bedoya-Rueda [a], Gustavo M. Paula-Santos [b,c], Sergio Caetano-Filho [a], Matheus Kuchenbecker [d,e], Humberto L.S. Reis [f], Ricardo I.F. Trindade [g]

[a] Universidade de São Paulo, Instituto de Geociências, Rua do Lago, 562, São Paulo 05508-080, Brazil
[b] Universidade de Campinas, Instituto de Geociências, Rua Carlos Gomes 255, Campinas 13083-855, Brazil
[c] Faculty of Geosciences and MARUM-Center for Marine Environmental Sciences, University of Bremen, Leobener Strasse 8, 28359, Bremen, Germany
[d] Universidade Federal dos Vales do Jequitinhonha e Mucuri, Instituto de Ciência e Tecnologia, Centro de Estudos em Geociências, Laboratório de Estudos Tectônicos, Rodovia MGT 367, Km 583, Diamantina 39100-000, Brazil
[e] Universidade Federal de Minas Gerais, Centro de Pesquisas Professor Manoel Teixeira da Costa, Av. Antônio Carlos, 6627, Belo Horizonte 31270-901, Brazil
[f] Universidade Federal de Ouro Preto, Departamento de Geologia-Escola de Minas, Laboratório de Modelagem Tectônica (LabMod), Campus Morro do Cruzeiro, Ouro Preto 35400-000, Brazil
[g] Universidade de São Paulo, Instituto de Astronomia, Geofísica e Ciências Atmosféricas, Rua do Matão, 1226, São Paulo 05508-090, Brazil

ARTICLE INFO

Article history:
Received 18 May 2020
Received in revised form 11 January 2021
Accepted 16 February 2021
Available online 26 February 2021
Editor: I.D. Somerville

Keywords:
Ediacaran-Cambrian
São Francisco Basin
Strontium isotopes
Foreland basin

ABSTRACT

The Bambuí Group is a marine sedimentary record of an intracratonic foreland basin developed at the terminal Ediacaran and early Cambrian during the assembly of West Gondwana. Here we present a basin-scale high-resolution Sr isotope stratigraphy for the basal Bambuí Group, aiming to understand the spatial and temporal variations of the $^{87}Sr/^{86}Sr$ ratios and to explore the controls over the Sr isotope system in intracontinental marine environments. Assessment of the stratigraphic evolution of both Sr concentrations and Sr isotopes shows a major increase in Sr/Ca ratios (up to 0.004) and a decrease in the $^{87}Sr/^{86}Sr$ ratios from 0.7086 to 0.7076 in the high stand system tract of the basal 2nd-order sequence. These changes precede a large positive $\delta^{13}C$ excursion typically found across the basin in the middle Bambuí Group. The high variability of both $^{87}Sr/^{86}Sr$ and Sr/Ca ratios was not caused by globally uniform changes in isotopic compositions of seawater, but rather likely reflect marine restriction and paleogeographic changes of the depositional environments at basin scale. This would result from the tectonic uplift of Neoproterozoic orogenic belts around the São Francisco craton, which generated an isolated foreland marine basin. Compared to the global ocean, such a smaller intracontinental reservoir would be more sensitive to the Sr isotope composition from the different rock sources. We suggest that changes on the balance between carbonate production and accommodation associated with tectonically-related flexural subsidence progressively modified the continental drainage patterns, sedimentary sources and the chemical weathering regimes, altering the strontium influxes and isotopic compositions of the seawater in the early Bambuí basin cycle. Similar anomalies in the strontium isotope record are also recorded in coeval marine basins across West Gondwana and suggest that tectonics might have played an important role on seawater chemistry at the Neoproterozoic-Paleozoic transition.

1. Introduction

The assumption that modern oceans are homogeneous with respect to $^{87}Sr/^{86}Sr$ ratios is based on the residence time of Sr (10^6 years) in this reservoir, which is far higher than its mixing time (10^3 years) and also in the efficient oceanic circulation patterns observed in the modern Earth's tectonic configuration (Elderfield 1986; Hodell et al. 1990; Veizer et al., 1989; Veizer et al. 1999; Krabbenhoft et al. 2010; McArthur et al. 2012). This fact has endorsed this isotopic proxy to be used to correlate marine sedimentary successions worldwide, especially in Precambrian sections where biostratigraphic data is scarce (Melezhik et al. 2001; Halverson et al. 2007, 2010; Krabbenhoft et al. 2010; McArthur et al. 2012; Kuznetsov et al. 2013). Moreover, considering the continental weathering regime and hydrothermal fluxes related to oceanic crust spreading as the main controls over this marine isotope system, the $^{87}Sr/^{86}Sr$ ratio is an essential tool for understanding the tectonic processes of the past and their impacts on marine ecosystems, habitats,

* Corresponding author.
E-mail address: guacaneme@usp.br (C. Guacaneme).

https://doi.org/10.1016/j.gr.2021.02.007
1342-937X/

biological diversity, and geochemical cycles (DePaolo and Ingram 1985; Chaudhuri and Clauer 1986; Palmer and Edmond 1989; Zaky et al. 2019).

In modern epicontinental basins, however, variations in climate and sea-level changes can strongly influence the $^{87}Sr/^{86}Sr$ record, and continental water inputs can locally modify the Sr isotope compositions of the basins (i.e., Ingram and Sloan 1992; Huang et al. 2011; Beck et al. 2013; Schildgen et al. 2014, Peucker-Ehrenbrink and Fiske 2019). For instance, on longer time scales, low $^{87}Sr/^{86}Sr$ ratios in the Miocene record of the Mediterranean Sea adjacent to the uplifting Alps and Apennines mountains, are attributed to a high influx of Sr from non-radiogenic $^{87}Sr/^{86}Sr$ Mesozoic carbonates in the hinterland coupled with restricted exchange of water with the global oceans (Schildgen et al. 2014). Therefore, the continental flux of Sr into the oceans does not necessarily have to be radiogenic but rather depends on changes in spatial distribution and the age of the exoreic continental bedrock, climate and drainage patterns through geological time (i.e., Peucker-Ehrenbrink and Fiske 2019).

The strontium isotope record of the Ediacaran-Cambrian marine carbonates from the Bambuí Group, in the São Francisco Basin, shows a potential link between major geochemical disturbances on the Sr budget and episodic restriction of the marine basin during Gondwana assembly (Paula-Santos et al. 2017). This sedimentary unit presents non-radiogenic $^{87}Sr/^{86}Sr$ ratios, mismatching those expected for the late Ediacaran and early Cambrian record (Melezhik et al. 2001; Halverson et al. 2010; Kuznetsov et al. 2013; Zaky et al. 2019). Additionally, a regional increase in Sr/Ca ratios is observed in the 2nd-order scale, preceding an extremely coupled positive $\delta^{13}C$ excursion (reaching values as high as +16‰ and − 14‰, for $\delta^{13}C_{carb}$ and $\delta^{13}C_{org}$, respectively; Iyer et al. 1995; Caetano-Filho et al., 2021), suggesting that tectonics and/or climate induced changes in seawater chemistry, triggering biochemical responses (Caetano-Filho et al., 2019, 2021).

Here, we present a basin-scale high-resolution Sr isotope stratigraphy for the basal Bambuí Group, aiming to understand the spatial and temporal variations of the $^{87}Sr/^{86}Sr$ ratios and explore the controls over the Sr isotope system in ancient intracontinental marine environments. We also aim to better understand how tectonic and climate changes may have impacted the biogeochemical cycles of the basin. Major paleogeographic reconfigurations, orogeneses and strong climatic oscillations had occurred at the Ediacaran-Cambrian transition, which are apparently linked to geochemical disturbances and to profound ecological innovations in the marine ecosystems (Knoll et al. 2006; Canfield et al. 2007; Hoffman et al. 1998; Hoffman and Schrag 2002; Campbell and Squire 2010; Young 2013; Reis and Suss 2016).

2. Geological setting

2.1. The São Francisco basin in West Gondwana

The São Francisco craton, together with the Congo craton, in western Africa, corresponds to the inner and most stable part of one of the continents involved in the assembly of West Gondwana supercontinent (Fig. 1B), during Neoproterozoic-Paleozoic transition (e.g. Alkmim et al. 2006; Heilbron et al. 2017). The craton is surrounded by diachronic Neoproterozoic mobile belts, namely Brasília (west), Araçuaí (east), Rio Preto, Riacho do Pontal and Sergipano (north) each one presenting a singular tectonic and structural history (e.g. Alkmim et al. 2017; Caxito et al. 2017; Valeriano 2017; and references therein).

As consolidated in the literature, the São Francisco basin (Fig. 1A) encompasses the various sedimentary units that cover a large part of the homonymous craton, representing in fact, a set of superposed sedimentary basins (e.g. Alkmim and Martins-Neto, 2001, Reis et al. 2017). These sedimentary units unconformably overly the Archean to Paleoproterozoic cratonic basement, and occur within three major structural domains: the Pirapora Aulacogen, a buried NW-trending graben at the central portion of the basin, and two basement highs, named Sete Lagoas and Januária, which bound this aulacogen to south and north, respectively (Fig. 1A).

At the end of the Neoproterozoic era, the São Francisco basin hosted the sediments of a complex foreland system developed on the São Francisco craton in response of the multiple loads exerted by the growth of the surrounding orogens (e.g. Martins-Neto 2005, 2009; Alkmim

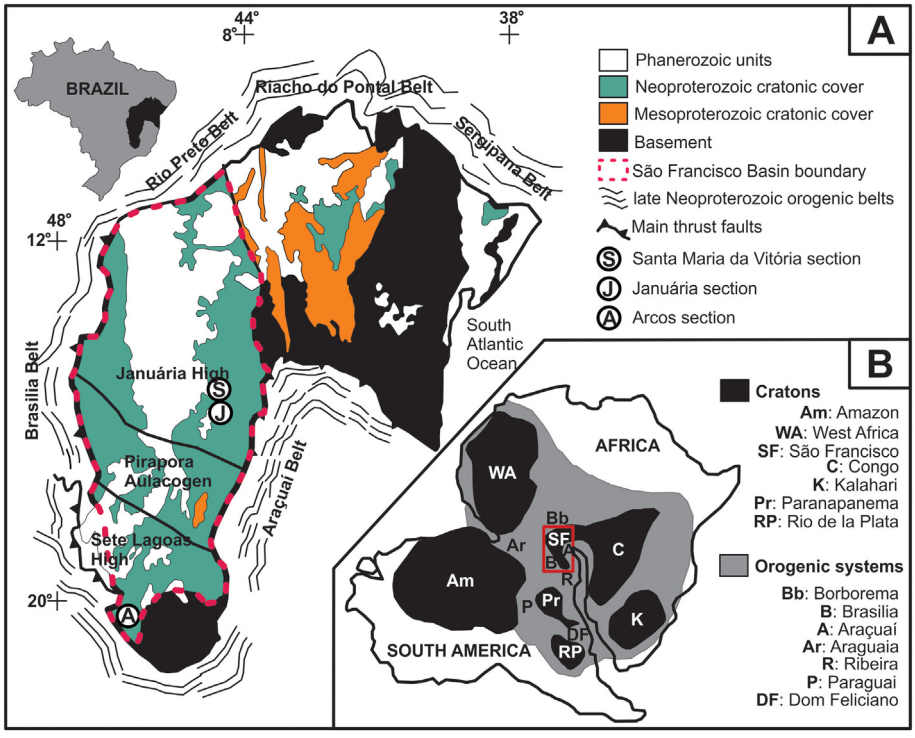

Fig. 1. A. Geological map of the São Francisco Basin (east-central Brazil) with location of stratigraphic sections. (modified from Caetano-Filho et al. 2019) B. Paleogeographic reconstruction of the late Neoproterozoic West Gondwana (modified from Alkmim et al. 2006).

et al. 2006; Alkmim and Martins-Neto 2012; Reis et al. 2016, 2017; Pimentel et al. 1999; Santos et al. 2000; Alkmim and Martins-Neto 2001; Reis and Suss 2016; Kuchenbecker et al. 2020). The rocks encompassed in the Bambuí Group are the remaining records of a late stage of such foreland system (Kuchenbecker et al. 2020).

The Bambuí Group consists of mixed carbonate-siliciclastic succession that can reach up to 3 km-thick in its main depocenter (Alkmim and Martins-Neto 2012; Martins-Neto 2009; Reis and Suss 2016; Reis et al. 2017; Caetano-Filho et al. 2019). The lithostratigraphic array of the group (Costa and Branco, 1961, Dardenne 1978) includes six basinwide formations (base to top): Carrancas (diamictite, pelite, dolomite), Sete Lagoas (limestone, dolomite, pelite), Serra de Santa Helena (pelite, limestone), Lagoa do Jacaré (limestone, pelite), Serra da Saudade (pelite, limestone) and Três Marias (sandstone, pelite). The Samburá (conglomerate) and Lagoa Formosa (conglomerate, pelite, dolomite) formations are restricted to the western border of the basin (Castro and Dardenne 2000; Uhlein et al. 2011; Uhlein et al. 2017), while the Jaíba (limestone) and Gorutuba (conglomerate, sandstone) formations occur only in its eastern border (Chiavegatto et al. 2003; Kuchenbecker et al. 2016b).

The occurrences of the index fossil *Cloudina* sp. (Warren et al. 2014; Perrella et al. 2017) and the presence of c. 550 Ma zircons (e.g. Paula-Santos et al. 2015; Kuchenbecker et al. 2020) in the Sete Lagoas Formation converge towards an Ediacaran-Early Cambrian age for the deposition of the Bambuí Group. This was reinforced by the dating of a tuff layer within Serra da Saudade Formation, which yielded the age of 520.2 ± 5.3 Ma (Moreira et al. 2020).

2.2. Sequence stratigraphy and chemostratigraphy of the basal Bambuí Group

In the last decades, many studies about the stratigraphic architecture and chemostratigraphic patterns of the Bambuí Group have been carried out to investigate the basin's evolution and paleoenvironmental conditions (e.g. Santos et al. 2000, 2004; Martins and Lemos 2007, Misi et al. 2007; Vieira et al., 2007a, b; Babinski et al. 2007; Caxito et al. 2012, 2018; Reis and Suss 2016; Alvarenga et al. 2014, Warren et al. 2014; Paula-Santos et al. 2015, 2017; Kuchenbecker et al. 2016a; Perrella et al. 2017; Guacaneme et al. 2017; Uhlein et al., 2017, 2019; Hippertt et al. 2019; Caetano-Filho et al., 2019, 2021).

The Bambuí Group has been envisaged as an unconformity-bounded 1st-order sequence, which encompasses four retrogradational-progradational 2nd order sequences (e.g. Martins and Lemos 2007, Reis and Suss 2016, Caetano-Filho et al. 2019, Uhlein et al. 2019). The focus of this paper is the basal 2nd order sequence, which has been the most studied interval of the basin.

From a chemostratigraphic perspective, Paula-Santos et al. (2017) divided the basal Bambuí Group in three Chemostratigraphic Intervals (CIs) based on $\delta^{13}C$ values and $^{87}Sr/^{86}Sr$ ratios (Fig. 2), which are associated with three different stages of the basin. Integrating the previous contributions, Caetano-Filho et al. (2019) presented a basin-scale sequence stratigraphy framework for the basal 2nd-order sequence of the Bambuí Group coupled to the chemostratigraphy patterns described by Paula-Santos et al. (2017). This framework is briefly described below.

The lowermost Bambuí 2nd-order sequence is up to a few hundreds of meters-thick, and comprises a basal transgressive system tract (TST) and a highstand systems tract (HST). The TST is formed by the coarse-grained siliciclastics of the Carrancas Formation grading upward into the carbonates and pelites of Sete Lagoas Formation, in a retrogradational stacking pattern (Vieira et al. 2007a; Kuchenbecker et al. 2013, 2016a; Reis et al. 2016; Caetano-Filho et al. 2019). This interval is bounded in the top by a maximum flooding surface and encompasses the CI-1 of Paula-Santos et al. (2017), which records a sharp increase of the $^{87}Sr/^{86}Sr$ ratios from 0.7074 to 0.7082 (e.g., Babinski et al. 2007). The TST cap carbonates commonly present aragonite pseudomorph fans

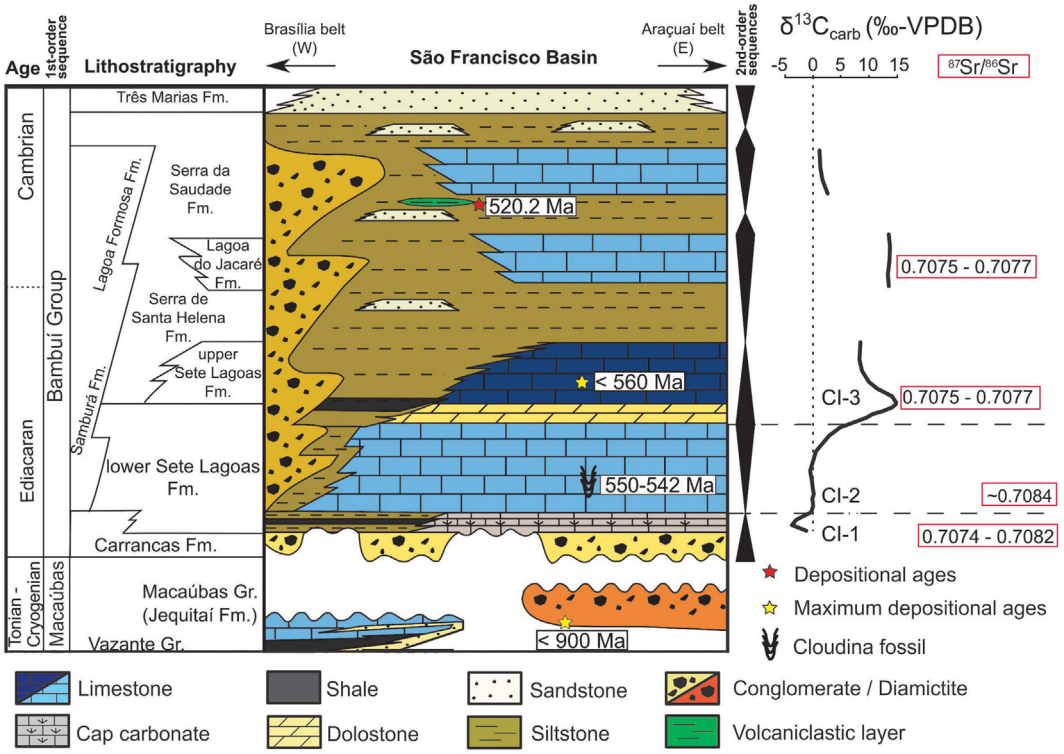

Fig. 2. Lithostratigraphic chart of the 1st-order Bambuí Sequence and chemostratigraphic evolution in the São Francisco Basin (modified from Caetano-Filho et al. 2019). *Cloudina* sp. index fossil defines a late Ediacaran age (lower Sete Lagoas Formation - Warren et al. 2014). Maximum depositional ages are represented by the yellow stars (Macaúbas Group – Babinski et al., 2012; upper Sete Lagoas Formation – Paula-Santos et al. 2015), depositional age of volcaniclastic layer is represented by the red star (upper Serra da Saudade Formation - Moreira et al. 2020). Chemostratigraphic Intervals (CI) from Paula-Santos et al. (2017).

and negative to positive $\delta^{13}C$ excursions from −5 to c. 0‰ (Santos et al. 2000; Babinski et al. 2007, Vieira et al. 2007b, 2015; Caxito et al. 2012, 2018; Alvarenga et al. 2014, Kuchenbecker et al. 2016a, Paula-Santos et al. 2015, 2017), which are typical features of Neoproterozoic post-glacial deposits (Hoffman et al. 1998; Hoffman and Schrag 2002). Sr contents of the TST carbonates are low (< 500 ppm), resulting in low average Sr/Ca ratio of 0.001 (Caetano-Filho et al. 2019).

The overlying highstand systems tract (HST) encompasses the carbonate-dominated successions of the basal to middle Sete Lagoas Formation (Reis and Suss 2016; Caetano-Filho et al. 2019). Defining a progradational pattern, the HST evolves from outer to inner carbonate ramp deposits (Reis and Suss 2016). This systems tract corresponds to most of the CI-2, which shows $\delta^{13}C$ values around 0‰ and $^{87}Sr/^{86}Sr$ ratios of ~0.7084 (Paula-Santos et al. 2017; Fig. 2). Considering the occurrence of the index fossil *Cloudina* sp. within this interval (Warren et al. 2014; Perrella et al. 2017) and the overall tectono-stratigraphic architecture of the Ediacaran-Cambrian strata, it has been proposed that the Bambuí inner sea was connected to the global ocean, allowing the strontium isotope homogenization and animal migration. An important basin-wide geochemical change in the Sr content and Sr/Ca ratios is observed within this HST, allowing its subdivision into a basal early highstand systems tract (EHST) and an upper late highstand systems tract (LHST) (Caetano-Filho et al. 2019).

The EHST is represented by dark-gray calcimudstones to bindstones with very low terrigenous contents, displaying slightly positive $\delta^{13}C$ values between 0 and + 1‰ right above the MFS, and a slight increase in the Sr content. Average Sr/Ca ratio remains similar to the lower TST around 0.001. This stratigraphic interval marks the stabilization of a marine carbonate ramp in the basal Bambuí sequence, with predominance of carbonate sedimentation (Caetano-Filho et al. 2019). The LHST presents mainly bindstones and peloidal calcimudstones deposited in mid- to inner ramp settings (Reis and Suss 2016; Caetano-Filho et al. 2019), whose chemostratigraphic features record major paleoenvironmental changes in the basin, probably enhanced seawater alkalinity (Paula-Santos et al. 2020). In the LHST, a remarkable increase in Sr content is observed, reaching up to 3500 ppm, and Sr/Ca ratios with an average value of 0.004. Such increase is not followed by a change in the carbonate facies through regressive systems tract, neither by any major increase in carbonate content. This interval is correlative to the *Cloudina* fossil interval of Warren et al. (2014).

An erosional unconformity locally associated with dolomitic layers and subaerial exposure features bounds the upper 2nd-order sequence boundary. This unconformity is overlain by the next retrogradational-progradational 2nd-order sequence, represented by the deposits of the uppermost Sete Lagoas Formation and the Serra de Santa Helena and Lagoa do Jacaré formations (Reis and Suss 2016; Caetano-Filho et al. 2019). The carbonate rocks of this sequence show an extreme positive $\delta^{13}C$ excursion that reach values as high as +16‰ (i.e., Iyer et al. 1995), with these unusual heavy carbon isotope compositions persisting throughout the 2nd-order sequence (Middle Bambuí Isotope Excursion; Uhlein et al. 2019; Caetano-Filho et al., 2021; Fig. 2). This interval corresponds to the CI-3 from Paula-Santos et al. (2017).

The $^{87}Sr/^{86}Sr$ ratios recorded in the CI-3 decrease to 0.7074–0.7076 (Caxito et al. 2012; Alvarenga et al. 2014; Paula-Santos et al. 2015, 2017) and deviate from the $^{87}Sr/^{86}Sr$ ratios around 0.7084 expected for late Ediacaran to early Cambrian carbonate successions (Melezhik et al. 2001; Halverson et al. 2010; Kuznetsov et al. 2013; Zaky et al. 2019). Thus, this interval might be interpreted as marking the increasingly restricted conditions of the Bambuí foreland system, caused by the continuous uplift of the surrounding orogenic belts. It would have culminated with a restricted or absent connection with global water reservoirs, limiting the water circulation and isotope system homogenization (Kuchenbecker et al. 2016a; Paula-Santos et al. 2017; Uhlein et al. 2019; Hippertt et al. 2019; Caetano-Filho et al. 2019).

3. Samples and methods

3.1. Studied sections

In this study, three stratigraphic sections of the basal Bambuí Group were described and sampled from different portions the São Francisco Basin, corresponding to the Arcos, Januária and Santa Maria da Vitória sections (Fig. 1A). Description of sedimentary facies, sequence stratigraphy framework, chemostratigraphy and correlation of these sections were previously presented by Kuchenbecker et al. (2016a) and Caetano-Filho et al. (2019). They encompass the two lowermost 2nd-order sequences from the Bambuí Group, recording the typical $\delta^{13}C$ and Sr/Ca ratios evolution presented in section 2.2. The stratigraphic correlation was based on the identification of two major stratigraphic surfaces (a maximum flooding surface and an unconformity) and stratigraphic stacking patterns (Figs. 3-5).

The Arcos section is a 175 m-thick continuous section obtained from drill-cores acquired at the southern portion of the basin (Figs. 1 and 3). It records the lowermost 2nd-order sequence from the Bambuí Group, represented by the Carrancas and Sete Lagoas formations unconformably overlying the Archean cratonic basement within the Sete Lagoas High. In this section, the TST is marked by a fining-upward pattern comprising basal diamictites that grade upward into intraclastic calcarenites and calcilutites, and then to marlstones and siltstones, which marks the MFS. These limestones present aragonite pseudomorph crystal fans and display negative $\delta^{13}C$ values of CI-1 (Kuchenbecker et al. 2016a; Paula-Santos et al. 2017; Caetano-Filho et al. 2019), which led to the interpretation of post-glacial cap carbonates formed under the influence of melted freshwaters (Kuchenbecker et al. 2016a). Upward, calcilutites grade into marlstones and siltstones that mark the MFS (Fig. 3). The EHST is defined by the transition of siltstones to intraclastic limestones that grade into a thick package of calcilutites with microbial lamination and interbedded shales, presenting a plateau of $\delta^{13}C$ values close to +1‰, matching the CI-2 (Kuchenbecker et al. 2016a; Paula-Santos et al. 2017; Caetano-Filho et al. 2019).

Within the microbial calcilutites interval, an abrupt increase in Sr/Ca ratios defines the LHST, ending with thick beds of coarse-grained dolostones and oolitic dolostones (Caetano-Filho et al. 2019). Intraclastic carbonate breccia layers mark the upper sequence boundary (SB1) Kuchenbecker et al. 2016a; Reis and Suss 2016; Caetano-Filho et al. 2019; Fig. 3). The dolostones grade upward into dark stromatolitic limestones with a large positive $\delta^{13}C$ excursion up to +8‰ and low Sr/Ca ratios in the overlying sequence (Kuchenbecker et al. 2016a; Caetano-Filho et al. 2019).

The Januária section is a 140 m-thick composite section encompassing the mixed carbonate-siliciclastic strata of the Sete Lagoas, Serra de Santa Helena and Lagoa do Jacaré formations exposed in the Januária basement High (Figs. 1 and 4). The TST displays pinkish to reddish limestones with microbial lamination and aragonite pseudomorphs, which unconformably overlie Archean-Paleoproterozoic basement assemblages and are marked by a negative to positive $\delta^{13}C$ excursion within their basal 5 m (CI-1; Paula-Santos et al. 2017; Caetano-Filho et al. 2019). An interval of reddish to light gray peloidal bindstones with more frequent pelite intercalations and $\delta^{13}C$ values around −1‰ marks the maximum flooding surface (Fig. 4).

Upward, the EHST comprises peloidal limestones with microbial laminations, hummocky cross-stratification and wavy bedding, displaying a slightly increase on $\delta^{13}C$ values from −1 to +1‰. In the LHST, peloidal calcilutites grade upward into intraclastic calcarenite layers and intraclastic carbonate breccia beds that are overlain by a intraclastic doloarenite marking the upper sequence boundary (Fig. 4). The $\delta^{13}C$ values remain stable and positive around +1‰ through the highstand systems tract (CI-2; Paula-Santos et al. 2017). Although no fossil remnants have been described, this interval is correlated to the C*loudina*-bearing interval described by Warren et al. (2014) and Perrella et al. (2017). The overlying 2nd-order sequence is represented

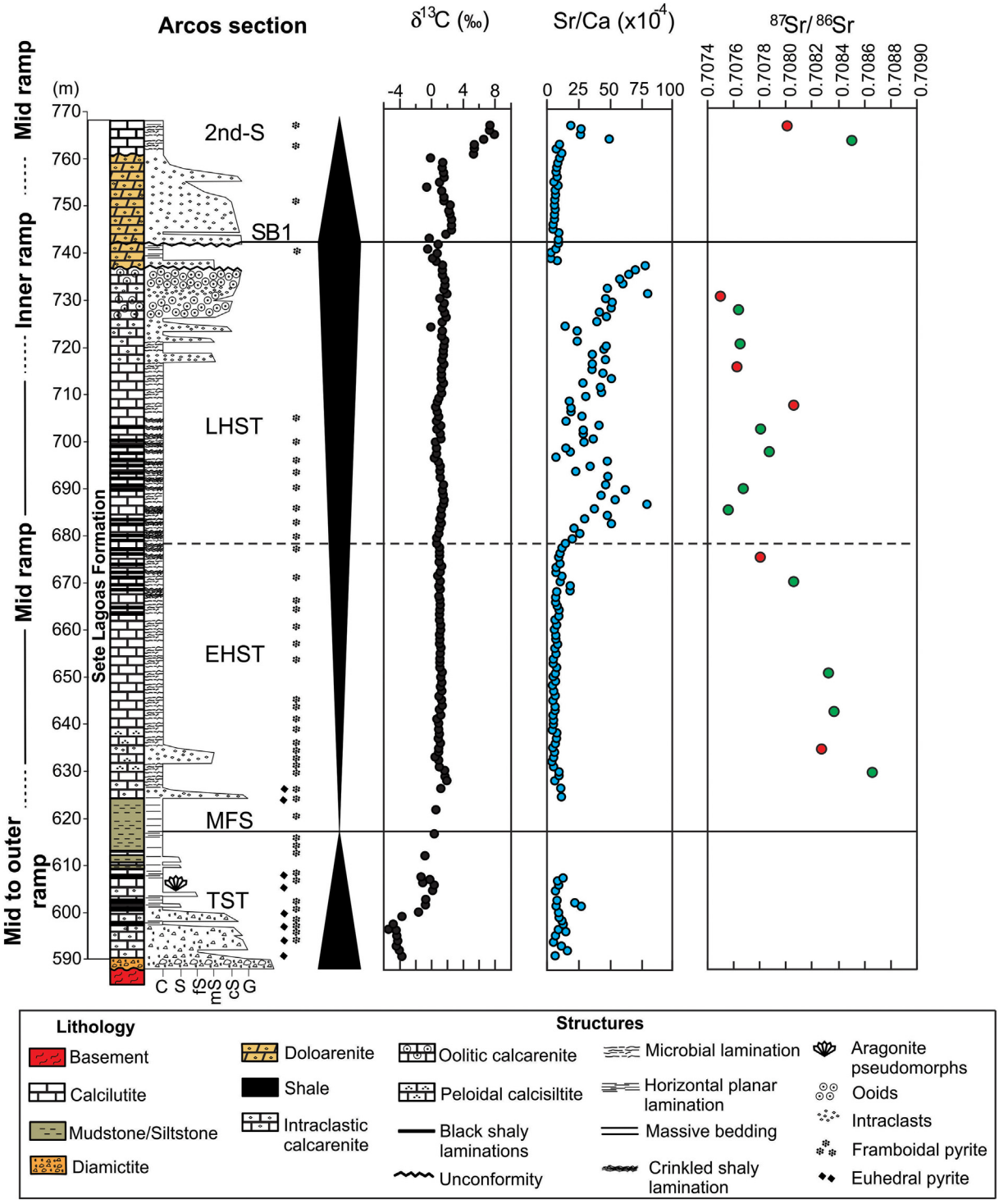

Fig. 3. Arcos section — integrated sequence stratigraphy and chemostratigraphy of $\delta^{13}C$ and Sr/Ca presented by Caetano-Filho et al. (2019), and new $^{87}Sr/^{86}Sr$ ratios. TST – Transgressive System Tract; MFS – Maximum Flooding Surface; EHST – Early Highstand System Tract; LHST – Late Highstand System Tract; SB1 – Sequence Boundary. Red dots represent $^{87}Sr/^{86}Sr$ ratios presented previously by Kuchenbecker et al. (2016a).

by mudstones and siltstones with planar laminations of the Serra de Santa Helena Formation and shallow water carbonate facies of the Lagoa do Jacaré Formation (Caetano-Filho et al. 2019). Positive $\delta^{13}C$ values ranging between +8 and + 12‰ support the correlation with the CI-3 of Paula-Santos et al. (2017).

The Santa Maria da Vitória section (SMV) is a composite section that comprises around a 150 m-thick carbonate-siliciclastic succession of the Sete Lagoas, Serra de Santa Helena and Lagoa do Jacaré formations overlying the cratonic basement on the northern Januária High (Figs. 1 and 5). In this section, the basal Bambuí transgressive systems tract is represented by 3 m-thick strata of white dolostones overlain by a thick succession of pinkish limestones with microbial lamination and sporadic occurrences of aragonite pseudomorphs. This interval displays in its basal 15 m the negative $\delta^{13}C$ excursion typical of the CI-1 (Paula-Santos et al. 2017). Pelitic layers interbedded with microbial limestones mark the maximum flooding surface (Fig. 5).

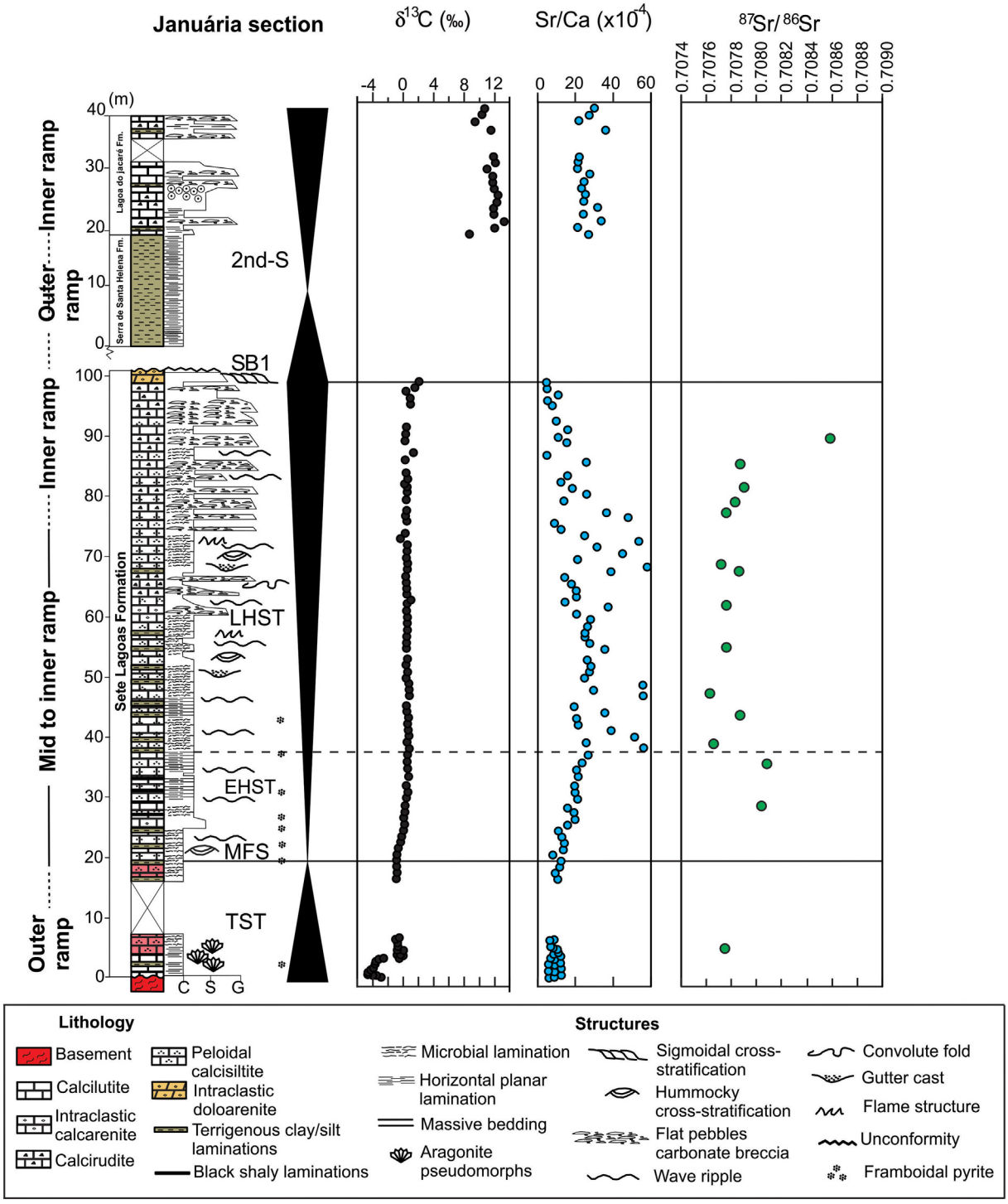

Fig. 4. Januária section — integrated sequence stratigraphy and chemostratigraphy of $\delta^{13}C$ values and Sr/Ca presented by Caetano-Filho et al. (2019), and new $^{87}Sr/^{86}Sr$ ratios- TST – Transgressive System Tract; MFS – Maximum Flooding Surface; EHST – Early Highstand System Tract; LHST – Late Highstand System Tract; SB1 – Sequence Boundary.

The overlying EHST is composed of microbial pinkish limestones with slightly negative $\delta^{13}C$ values (−1 to 0‰) that grade into gray limestones with hummocky cross-stratification, wavy bedding and restricted carbonate breccias, presenting slightly positive $\delta^{13}C$ values around +1‰. Sr/Ca ratios notably increase within the gray limestone interval marking the LHST interval (Fig. 5). A possible paleosol layer marks the sequence boundary (SB1) accompanied by a discontinuity in the $\delta^{13}C$ profile. The overlaying 2nd-order sequence starts with dolostones presenting microbial laminations and tepee-like structures of the uppermost Sete Lagoas Formation succeeded by siltstones and interbedded oolitic limestone layers of the Serra de Santa Helena Formation (Fig. 5). A remarkable increase on $\delta^{13}C$ values from +2 to +14‰ is observed in these strata (CI-3, Paula-Santos et al. 2017).

3.2. Strontium isotope analyses

Sixty-three carbonate samples distributed along the three studied sections were selected for Sr isotope analyses (Table 1), based on

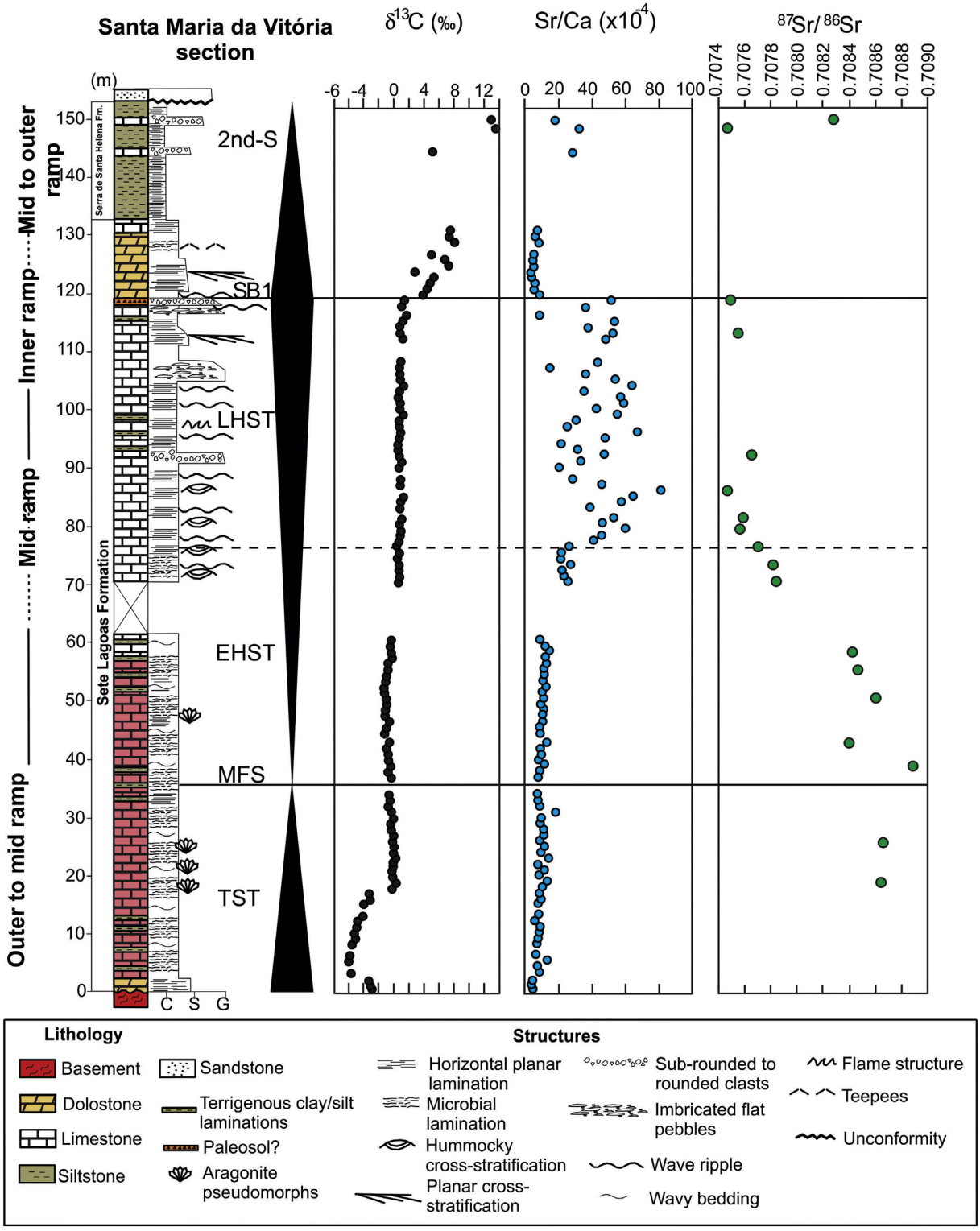

Fig. 5. Santa Maria da Vitória section — integrated sequence stratigraphy and chemostratigraphy of $\delta^{13}C$ values and Sr/Ca presented by Caetano-Filho et al. (2019), and new $^{87}Sr/^{86}Sr$ ratios. TST – Transgressive System Tract; MFS – Maximum Flooding Surface; EHST – Early Highstand System Tract; LHST – Late Highstand System Tract; SB1 – Sequence Boundary.

previously bulk rock samples analyzed for Sr and Ca using X-ray fluorescence, as well as stratigraphic-chemostratigraphic framework and sedimentology (Caetano-Filho et al. 2019). Petrographic analyses were carried out to identify depositional fabrics and sedimentary structures, and select the more preserved areas to obtain carbonate powder. A sequential leaching method was applied to systematically isolate least-altered carbonate phases from detrital siliciclastic Sr contamination (e.g., Li et al. 2011; Paula-Santos et al. 2017; Bellefroid et al. 2018), increasing the reliability of the results as a representative proxy of seawater.

Strontium isotope compositions were analyzed through the reaction of 100 mg of carbonate powder with 2.0 mL of HCl 0.1 N for one hour. The supernatant was discarded, and the sample was centrifuged and washed three times with Milli-Q water, also discarding the supernatant

Table 1
Sr contents, geochemical ratios and $^{87}Sr/^{86}Sr$ ratios of carbonates from the basal Bambuí Group at the Arcos, Januária and Santa Maria da Vitória sections.

Section	Sample	(m)	Tract	Lithology	Sr (μg/g)	Rb/Sr	Mn/Sr	Fe/Sr	Mg/Ca	Sr/Ca	$^{87}Sr/^{86}Sr$	erro (2σ)
Arcos	M-4	592.0	TST	Calcarenite	402	0.00158	1.235	24.978	0.367	0.0018	0.717756	0.000020
	M-12	599.3	TST	Calcarenite	890	0.00078	0.559	0.874	0.012	0.0028	0.711227	0.000016
	M-18*	604.8	TST	Calcarenite	174	0.06322	n.a.	n.a.	n.a.	n.a.	0.715348	0.000048
	M-20*	606.5	TST	Calcilutite	292	0.04795	n.a.	n.a.	n.a.	n.a.	0.709992	0.000008
	k-24a	613.0	TST	Calcilutite	760	0.00103	0.450	4.829	0.050	0.0021	0.710085	0.000017
	M-28	631.2	EHST	Calcisiltite	365	0.00050	0.087	0.464	0.033	0.0014	0.708663	0.000016
	M-29*	636.0	EHST	Calcisiltite	304	0.02303	0.329	2.531	0.013	0.0008	0.708271	0.000042
	K-30c	644.0	EHST	Calcilutite	308	0.00038	0.053	0.228	0.012	0.0010	0.708368	0.000020
	K-32a	652.0	EHST	Calcilutite	370	0.00025	0.035	0.661	0.025	0.0012	0.708326	0.000017
	M-36*	671.4	EHST	Calcilutite	598	0.00061	0.029	0.374	0.010	0.0012	0.708057	0.000020
	M-37*	676.4	EHST	Calcilutite	414	0.00725	0.242	0.725	0.014	0.0011	0.707804	0.000022
	M-39	686.7	LHST	Calcilutite	3950	0.00005	0.001	0.030	0.005	0.0108	0.707551	0.000019
	M-40*	690.9	LHST	Calcilutite	2538	0.00012	0.002	0.037	0.003	0.0051	0.707683	0.000072
	K-41b	698.7	LHST	Calcilutite	816	0.00014	0.005	0.060	0.005	0.0025	0.707872	0.000018
	K-42b	703.4	LHST	Calcilutite	1132	0.00007	0.002	0.050	0.003	0.0032	0.707799	0.000019
	M-45*	716.4	LHST	Calcilutite	1817	0.00055	0.055	0.154	0.003	0.0046	0.707622	0.000040
	M-46*	721.4	LHST	Calcilutite	1957	0.00051	0.051	0.358	0.003	0.0050	0.707648	0.000023
	K-43b	708.4	LHST	Calcilutite	863	0.00008	0.006	0.059	0.003	0.0030	0.708055	0.000018
	K-47b	728.4	LHST	Calcarenite	2643	0.00003	0.006	0.011	0.003	0.0089	0.707628	0.000017
	M-48*	731.4	LHST	Calcarenite	3304	0.00009	0.030	0.085	0.002	0.0083	0.707493	0.000020
	K-49c	738.9	LHST	Doloarenite	97	0.00050	1.436	6.235	0.524	0.0006	0.712481	0.000016
	K-52b	754.2	LHST	Doloarenite	268	0.00125	0.149	0.825	0.372	0.0016	0.712144	0.000020
	M-54	762.2	LHST	Doloarenite	188	0.00219	0.488	2.876	0.467	0.0008	0.713115	0.000019
	M-D6	764.2	2nd-S	Calcilutite	2094	0.00022	0.019	0.090	0.042	0.0078	0.708507	0.000018
	M-55*	767.2	2nd-S	Calcilutite	678	0.03687	n.a.	n.a.	n.a.	n.a.	0.708009	0.000022
Januária	CM-02	1.2	TST	Calcilutite	361	0.00186	1.097	1.770	0.008	0.0010	0.709710	0.000020
	CM-03	2.2	TST	Calcilutite	234	0.00383	4.088	2.656	0.007	0.0005	0.711768	0.000018
	CM-03f	3.2	TST	Calcilutite	3917	0.00011	0.162	0.072	0.006	0.0104	0.707740	0.000018
	CM-03 h	3.9	TST	Calcilutite	380	0.00203	0.409	1.081	0.016	0.0010	0.709170	0.000021
	CM-06a	6.3	TST	Calcisiltite	353	0.00196	0.497	2.312	0.047	0.0009	0.710316	0.000019
	CM-09	18.5	TST	Calcisiltite	450	0.00119	0.182	1.482	0.031	0.0011	n.a.	n.a.
	CM-10	19.5	TST	Calcisiltite	467	0.00139	0.149	1.653	0.027	0.0014	0.709797	0.000019
	CM-14	23.5	EHST	Calcisiltite	562	0.00074	0.137	1.236	0.042	0.0017	n.a.	n.a.
	CM-18	27.5	EHST	Calcisiltite	822	0.00011	0.009	0.125	0.017	0.0027	0.708020	0.000016
	CM-22	31.9	EHST	Calcisiltite	1092	0.00018	0.008	0.154	0.019	0.0029	n.a.	n.a.
	CM-24	34.7	EHST	Calcisiltite	952	0.00013	0.006	0.131	0.029	0.0032	0.708055	0.000019
	CM-27	38.1	LHST	Calcisiltite	2878	0.00002	0.002	0.016	0.004	0.0068	0.707644	0.000020
	CM-32	43.1	LHST	Calcisiltite	1056	0.00010	0.008	0.100	0.010	0.0027	0.707855	0.000021
	CM-35	46.8	LHST	Calcisiltite	2558	0.00003	0.002	0.027	0.005	0.0077	0.707622	0.000020
	CM-42	54.5	LHST	Calcisiltite	1446	0.00003	0.004	0.039	0.005	0.0040	0.707741	0.000018
	BAR-12	61.7	LHST	Calcisiltite	1724	0.00016	0.015	0.103	0.003	0.0031	0.707740	0.000019
	BAR-18	67.5	LHST	Calcarenite	1832	0.00006	0.012	0.075	0.005	0.0039	0.707845	0.000017
	BAR-19	68.5	LHST	Calcarenite	2637	0.00008	0.006	0.059	0.004	0.0070	0.707701	0.000017
	BAR-28	77.3	LHST	Calcarenite	2224	0.00010	0.015	0.050	0.004	0.0046	0.707742	0.000018
	BAR-29	79.1	LHST	Calcarenite	778	0.00011	0.028	0.115	0.013	0.0018	0.707814	0.000018
	BAR-32	81.7	LHST	Calcarenite	872	0.00004	0.019	0.049	0.013	0.0022	0.707883	0.000017
	BAR-35	85.7	LHST	Calcarenite	1080	0.00009	0.023	0.095	0.018	0.0029	0.707851	0.000017
	BAR-38	89.9	LHST	Calcarenite	438	0.00003	0.049	0.112	0.014	0.0012	0.708538	0.000018
	BAR-42	95.9	LHST	Calcarenite	n.a.	n.a.	n.a.	n.a.	n.a.	n.a.	0.709604	0.000016
Santa Maria da Vitória	COR-02	1.5	TST	Dolostone	103	0.00322	2.827	23.143	0.508	0.0005	0.710511	0,000020
	COR-05	4.5	TST	Calcilutite	234	0.00366	1.669	2.652	0.027	0.0006	0.713400	0,000018
	COR-07	6.5	TST	Calcilutite	181	0.00228	1.168	0.721	0.009	0.0005	0.709219	0.000021
	COR-11	11.3	TST	Calcilutite	252	0.00197	1.716	0.779	0.009	0.0007	0.709148	0.000019
	COR-15	16.0	TST	Calcilutite	282	0.00101	1.099	4.498	0.105	0.0011	0.709093	0.000016
	COR-18	19.0	TST	Calcilutite	456	0.00067	0.411	1.587	0.075	0.0011	0.708572	0.000016
	COR-25	26.0	TST	Calcilutite	293	0.00091	0.339	0.349	0.007	0.0008	0.708589	0.000018
	ALD-06	39.0	EHST	Calcilutite	408	0.00065	0.280	1.138	0.027	0.0009	0.708801	0.000019
	ALD-10	43.0	EHST	Calcilutite	446	0.00075	0.310	1.044	0.025	0.0009	0.708346	0.000017
	ALD-17	50.6	EHST	Calcilutite	552	0.00058	0.131	1.202	0.032	0.0012	0.708531	0.000018
	ALD-22	55.6	EHST	Calcilutite	396	0.00065	0.199	2.904	0.080	0.0013	0.708408	0.000016
	ALD-25	58.6	EHST	Calcilutite	469	0.00055	0.181	1.152	0.022	0.0012	0.708364	0.000016
	ALD-28	70.6	EHST	Calcilutite	1087	0.00007	0.013	0.059	0.008	0.0022	0.707816	0.000021
	ALD-31	73.6	EHST	Calcilutite	1209	0.00010	0.011	0.063	0.007	0.0027	0.707791	0.000019
	ALD-34	76.6	EHST	Calcilutite	1176	0.00010	0.016	0.076	0.005	0.0025	0.707687	0.000017
	ALD-37	79.6	LHST	Calcilutite	3947	0.00003	0.001	0.011	0.004	0.0081	0.707559	0.000016
	ALD-39	81.6	LHST	Calcilutite	2297	0.00003	0.005	0.022	0.005	0.0048	0.707576	0.000018
	ALD-43	86.3	LHST	Calcilutite	4099	0.00004	0.001	0.018	0.003	0.0084	0.707465	0.000019
	ALD-48	92.3	LHST	Calcilutite	1997	0.00002	0.005	0.019	0.005	0.0041	0.707640	0.000016
	BA-16	113.3	LHST	Calcilutite	2070	0.00002	0.001	0.010	0.004	0.0040	0.707539	0.000018
	BA-21	118.8	LHST	Calcilutite	2835	0.00001	0.001	0.002	0.003	0.0059	0.707486	0.000019
	BA-22	119.8	2nd-S	Dolostone	199	0.00039	0.236	1.229	0.528	0.0008	0.710041	0.000019
	BA-27	124.8	2nd-S	Dolostone	87	0.00018	2.541	3.827	0.527	0.0004	0.709446	0.000017
	BA-30	128.8	2nd-S	Dolostone	311	0.00068	0.513	6.288	0.409	0.0011	0.711044	0.000016
	BA-32	130.8	2nd-S	Dolostone	164	0.00230	1.414	19.577	0.548	0.0007	0.710846	0.000017
	BA-33	144.3	2nd-S	Calcisiltite	701	0.00098	1.290	1.139	0.267	0.0024	0.708736	0.000017

Table 1 (*continued*)

Section	Sample	(m)	Tract	Lithology	Sr (μg/g)	Rb/Sr	Mn/Sr	Fe/Sr	Mg/Ca	Sr/Ca	$^{87}Sr/^{86}Sr$	erro (2σ)
	BA-34	148.3	2nd-S	Calcisiltite	1367	0.00005	0.010	0.038	0.005	0.0024	0.707465	0.000019
	BA-35	149.8	2nd-S	Calcisiltite	705	0.00013	0.025	0.047	0.004	0.0017	0.708225	0.000018

Notes: *Sample data from Kuchenbecker et al. (2016a).
n.a. — not analyzed.

from each wash. Subsequently, ~3.0 mL of HCl 0.1 N was added into the dried sample for reaction through one hour. Again, the sample was centrifuged for 15 min, the supernatant transferred to Savillex and washed three times with Milli-Q water. This solution is the second leachate (L2) that underwent Sr purification process by the ion exchange chromatography technique, using a Sr-spec resin and HNO_3 as eluant. The $^{87}Sr/^{86}Sr$ ratios were measured in the TRITON thermal ionization mass spectrometer (TIMS, Thermo Fisher, Germany) at the Geochronological Research Center (CPGeo) of the University of São Paulo, Brazil. The ratios were normalized to $^{86}Sr/^{88}Sr = 0.1194$ in order to correct variable mass fractionation. The average value of the NBS-987 standard measured during analyses was 0.710250 ± 0.000018, ($n = 6$), and the Sr analytical blanks were generally below 28 pg.

3.3. Elemental geochemistry

For major and trace element mass fraction measurements, small pieces of carbonate samples devoid of terrigenous laminae and post-depositional features were carefully powdered in an agate mortar. The same leaching procedure used for Sr isotope analyses was performed and only the second leachate (L2) was analyzed. After drying L2 solution on a hot plate, the residue was converted into nitrates by adding 0.5 mL of concentrated HNO_3. This solution was evaporated and the residue was dissolved in 1% (*v*/v) HNO_3. Concentrations of Rb, Sr, Mn, Fe, Mg and Ca of carbonate fractions were measured by quadrupole inductively coupled plasma mass spectrometry (Q-ICP-S) using a X-Series (Thermo Fisher, Germany) mass spectrometer at the Laboratory of Isotope Geology of the Institute of Geosciences of the University of Campinas, Brazil.

4. Results

Strontium isotope compositions, element mass fractions and geochemical ratios of carbonates of the basal Bambuí Group are presented in Table 1, and primary $^{87}Sr/^{86}Sr$ ratios (selected in the item 5.1) are presented in Figs. 3, 4 and 5.

Carbonate samples from the Arcos section display very radiogenic $^{87}Sr/^{86}Sr$ ratios within the lowermost TST, between 0.7100 and 0.7177, and presents Sr content from 400 to 900 μg/g and Sr/Ca between 0.0018 and 0.0028 (Table 1). The $^{87}Sr/^{86}Sr$ ratios decrease progressively from 0.7087 to 0.7078 towards the top of EHST (Fig. 3), with Sr content varying from 300 to 600 μg/g and Sr/Ca ratios from 0.0008 to 0.0014 (Table 1). At the lower to middle LHST, $^{87}Sr/^{86}Sr$ ratios increase from 0.7075 to 0.7080, then decreasing to values around 0.7076 at the uppermost highstand systems tract (Fig. 3), accompanied by high strontium contents between 800 and 4000 μg/g, and high Sr/Ca ratios from 0.0025 to 0.001 (Table 1). Dolomites from the top this interval show very radiogenic $^{87}Sr/^{86}Sr$ ratios (> 0.7121), with low Sr contents and Sr/Ca ratios below 270 μg/g and 0.0016, respectively (Table 1). Carbonates from the basal portion of the overlying 2nd-order sequence show $^{87}Sr/^{86}Sr$ ratios between 0.7080 and 0.7085 (Fig. 3), with Sr contents varying from 600 to 2000 μg/g and Sr/Ca ratios of 0.0078 (Table 1). Geochemical contents recorded in this section show Rb/Sr ratios between 0.00005 and 0.00100, Mn/Sr between 0.001 and 1.500, Fe/Sr ranging from 0.01 to 24.98, and Mg/Ca ratios between 0.003 and 0.500 (Table 1).

In the Januária section, the $^{87}Sr/^{86}Sr$ ratios are also very radiogenic at the lowermost TST, with values up to 0.7117, and Sr contents and Sr/Ca ratios varying from 360 to 500 μg/g and 0.0005 to 0.0014, respectively (Table 1). However, one sample at the base of the Januária section (CM-03f) shows very low $^{87}Sr/^{86}Sr$ ratio of 0.7077, which is associated with high Sr mass fraction (~3920 μg/g) and aragonite pseudomorph crystal fans (Table 1, Fig. 4). Carbonate rocks of the EHST show $^{87}Sr/^{86}Sr$ ratios around 0.7080 (Fig. 4), and an upward progressive increase in Sr contents and Sr/Ca ratios from 500 to 1100, and from 0.0017 to 0.0032, respectively (Table 1). $^{87}Sr/^{86}Sr$ ratios from the LHST vary between 0.7076 and 0.7078, and increase to 0.7085 at the topmost portion (Fig. 4), presenting Sr contents from 430 to 2800 μg/g, and Sr/Ca ratios between 0.0012 and 0.0077 (Table 1). The carbonate successions of the Januária section show Rb/Sr ratios ranging from 0.00002 to 0.00300, Mn/Sr between 0.002 and 4.100, Fe/Sr varying from 0.02 to 2.66, and Mg/Ca ratios between 0.003 and 0.470 (Table 1).

Limestones of the Santa Maria da Vitória section display very radiogenic $^{87}Sr/^{86}Sr$ ratios at the lower TST between 0.7091 and 0.7134 (Fig. 5), associated to low Sr contents between 100 and 500 μg/g, and low Sr/Ca ratios from 0.0005 to 0.0010 (Table 1). Also, two samples from this interval (COR-18 and COR-25) show $^{87}Sr/^{86}Sr$ ratios around 0.7086 and present aragonite pseudomorphs (Table 1, Fig. 5). In the EHST, the $^{87}Sr/^{86}Sr$ ratios decrease upward, from 0.7088 to 0.7077 (Fig. 5), coupled to an increase in the Sr content from 400 to 1200 μg/g, and Sr/Ca ratios from 0.0009 to 0.0027 (Table 1). At the LHST, $^{87}Sr/^{86}Sr$ ratios are dominantly around 0.7075 (Fig. 5), and associated with high Sr contents between 2000 and 4000 μg/g, and high Sr/Ca ratios from 0.0040 to 0.0090 (Table 1). At the basal portion of the LHST, the $^{87}Sr/^{86}Sr$ and Sr/Ca ratios seem to define-untithetical trends, with non-radiogenic ratios associated with high Sr/Ca ratios (Fig. 5). Carbonates from the second 2nd-order sequence show $^{87}Sr/^{86}Sr$ ratios between 0.7074 and 0.7087 (Fig. 5), with Sr contents from 700 to 1400 μg/g, and Sr/Ca ratios from 0.0017 to 0.0024 (Table 1). Dolomites from this interval exhibit very radiogenic $^{87}Sr/^{86}Sr$ ratios between 0.7094 and 0.7121, with low Sr contents and Sr/Ca ratios less 300 μg/g and 0.0011, respectively (Table 1). This section shows Rb/Sr ratios between 0.00003 and 0.00360, Mn/Sr between 0.001 and 2.800, Fe/Sr ranging from 0.002 to 23.100, and Mg/Ca ratios between 0.003 and 0.550 (Table 1).

5. Discussion

5.1. Assessing post-depositional alteration and carbonate diagenesis

During post-depositional rock/fluid interaction such as meteoric-water diagenesis and dolomitization, carbonate minerals usually incorporate more Mn and Fe, accompanied by a decrease in the $\delta^{18}O$ values and in Sr concentrations, as well as an increase in $^{87}Sr/^{86}Sr$ ratios (Brand and Veizer 1980, 1981; Veizer et al. 1983; Banner and Hanson 1990; Jacobsen and Kaufman 1999; Melezhik et al. 2001; Brand 2004; Halverson et al. 2007; Derry 2010). Based on these observations, several studies have proposed systematic geochemical screenings based on elemental and isotope proxies to evaluate the original seawater signature and the post-depositional alteration on $^{87}Sr/^{86}Sr$ ratios of marine carbonates (i.e., Banner and Hanson 1990; Derry et al. 1992; Montañez et al. 1996, 2000; Jacobsen and Kaufman 1999; Melezhik et al. 2001; Fölling and Frimmel 2002; Halverson et al. 2007, 2010; Kuznetsov et al. 2013; Zaky et al. 2019). $^{87}Sr/^{86}Sr$ vs. Mn/Sr and Fe/Sr diagrams, as well as Mg/Ca ratios are often deployed to such task.

These works attempted to define "cut-off" values for these elements and geochemical ratios in order to determine the reliability of a given isotope dataset to record a primary marine signal of the Neoproterozoic seawater (i.e., Asmeron et al. 1991; Kaufman et al. 1993; Kaufman and

Knoll 1995; Kuznetsov et al. 1997; Jacobsen and Kaufman 1999; Fölling and Frimmel, 2002; Kuznetsov et al. 2013). However, such works relied on limited number of samples, usually from a single stratigraphic unit or from sedimentary units that share similar geologic histories. This resulted in very discrepant cut-off values, which means they may not be suitable for all ancient carbonate successions deposited under different environmental conditions (i.e., Paula-Santos et al. 2017; Zaky et al. 2019).

Additionally, the identification of stratigraphic levels with high Sr concentrations on the Bambuí Group can introduce a bias in the geochemical analysis of post-depositional processes. Paula-Santos et al. (2017) show that most of the considered pristine $^{87}Sr/^{86}Sr$ ratios were selected from these Sr-rich carbonates, with the more radiogenic ratios from the EHST and TST being discarded, though some of them were in accordance with ratios expected for the late Ediacaran. Caetano-Filho et al. (2019) argued the basin-wide increase in Sr mass fractions and Sr/Ca ratios are non-facies dependent feature, which might indicate a paleoenvironmental change in the basin resulting in increased incorporation of Sr in the carbonate lattice. This shows that the difference in Sr mass fractions across the basal 2nd-order sequence of the Bambuí Group are probably environmental driven, rather than a post-depositional artifact.

To avoid misuse of pre-established cut-off values and introduction of such bias, instead of fixed numerical values, we carefully evaluate Sr isotope ratios from each stratigraphic interval from the Bambuí Group, we follow Paula-Santos et al. (2017) who suggest that these values should be dynamic and determined according to regional chemostratigraphy.

For the lowermost TST, the dominant very radiogenic $^{87}Sr/^{86}Sr$ ratios from 0.7090 to 0.7177 are associated with high geochemical ratios of Rb/Sr, Mn/Sr, Fe/Sr and Mg/Ca for most of carbonate samples of this interval. In contrast, some carbonate samples display lower Sr ratios between 0.7075 and 0.7077, which are associated to lower geochemical ratios, as well as to aragonite pseudomorphs and higher Sr contents (Fig. 6). Sample COR-25 from SMV section also has a lower $^{87}Sr/^{86}Sr$ ratio of 0.7086 coupled to lower elemental ratios (Table 1). These ratios between 0.7075 and 0.7086 are consistent with those reported by Paula-Santos et al. (2017) for the basal cap carbonates and we also considered them as the most representative of seawater composition for the TST. The more radiogenic ratios are considered altered.

Carbonates with $^{87}Sr/^{86}Sr$ ratios >0.7090 from the TST could record a mixing between less radiogenic seawater and radiogenic freshwater, which diminished as transgression progressed increasing the relative proportion of the geochemical marine patterns. This is supported by flat rare earth element patterns that suggest a large input of

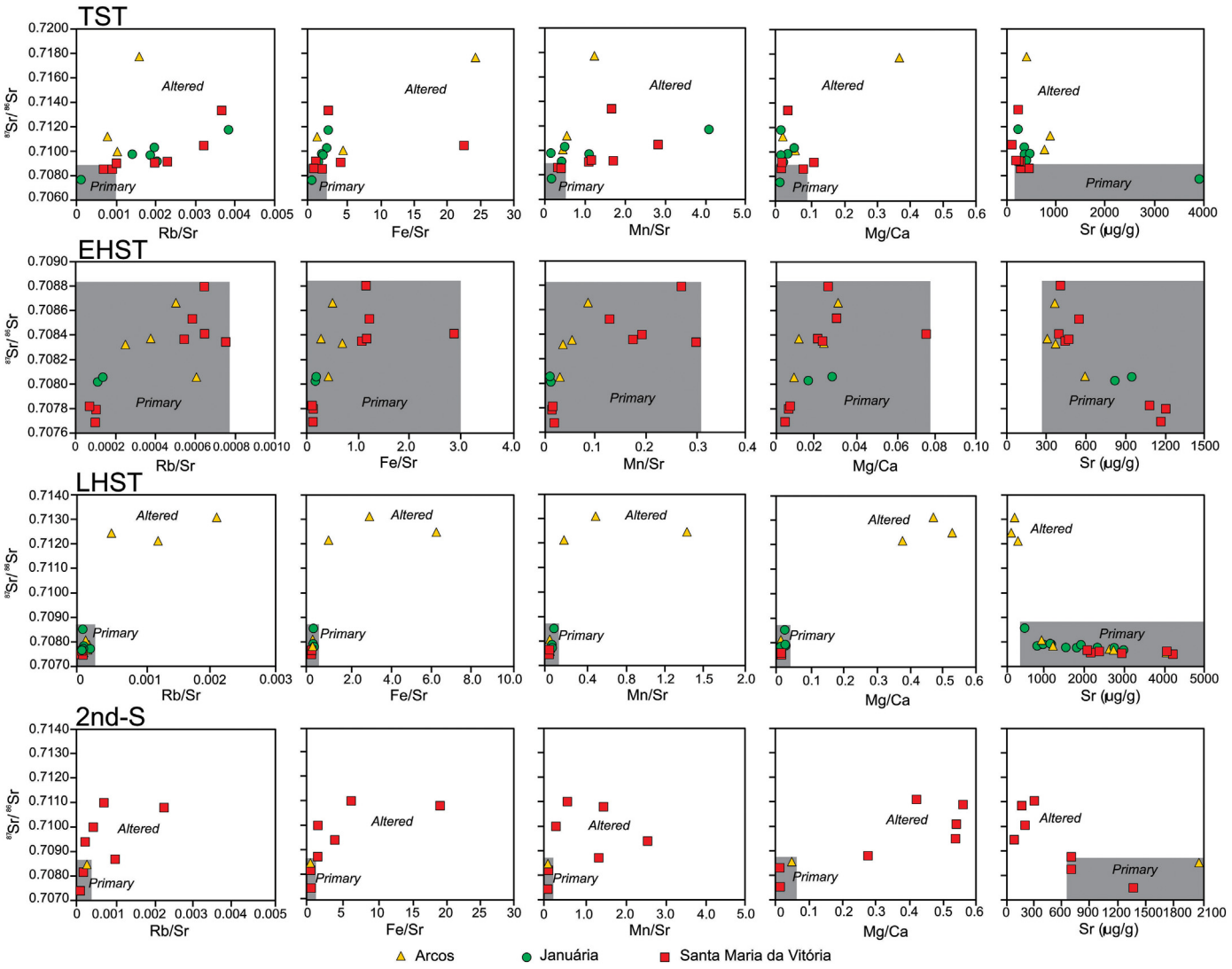

Fig. 6. Cross-plot diagrams of $^{87}Sr/^{86}Sr$ ratios vs. geochemical ratios of Rb/Sr, Fe/Sr, Mn/Sr, Mg/Ca and Sr contents for the systems tracts (TST, EHST, LHST and 2nd-S) of the basal Bambuí Sequence. Primary $^{87}Sr/^{86}Sr$ ratios are inside the gray square.

freshwater/meltwater mixed to seawater during transgression, and is consistent with a post-glacial scenario for the TST (i. e., Shields 2005, Liu et al. 2014, Kuchenbecker et al. 2016a; Wei et al. 2019, Paula-Santos et al., 2018, 2020). In any case, they are not considered in our geological discussion.

Strontium isotope ratios for the EHST range from 0.7077 to 0.7088 and show a positive correlation with geochemical ratios of Rb/Sr, Mn/Sr, Fe/Sr and Mg/Ca (Fig. 6), which would suggest a diagenetic trend towards the higher $^{87}Sr/^{86}Sr$ ratios (Banner and Hanson 1990; Jacobsen and Kaufman 1999; Fölling and Frimmel 2002; Halverson et al. 2007; Alvarenga et al. 2014; Kuchenbecker et al. 2016a; Paula-Santos et al. 2017). However, we note that an upward decreasing trend of the ratios is observed in all studied sections, preceding the increase in the Sr/Ca at the LHST. If such recurrent feature basin-wide were to be a post-depositional feature it would require a diagenetic overprint of basinal scale that we find unlikely due the lack of petrographical evidence. Also, since this drop down in the Sr isotope ratios precedes a very well describe major environmental change in the basin, we find it more reasonable that they are the record of a progressive change in seawater chemistry, rather than any diagenetic overprint. In addition, geochemical ratios are extremely low ($Rb/Sr < 0.008$, $Mn/Sr < 0.3$ and $Fe/Sr < 3$) for this interval in all the sections (Table 1) and there is no significant variation in Rb, Mn, and Fe mass fractions of the EHST samples. At the light of these evidences we argue that these Sr isotope ratios are pristine and that the decrease in these isotope ratios reflects basin-scale paleoenvironmental changes, rather than pointing to basin wide diagenetic processes restricted to the EHST strata.

For the LHST, the $^{87}Sr/^{86}Sr$ ratios vary between 0.7074 and 0.7131 (Fig. 6) and, in dolomites, presents a systematic correlation with Rb/Sr, Mn/Sr, Fe/Sr and Mg/Ca ratios, indicating post-depositional alteration of the more radiogenic isotope ratios higher than 0.7085 (i.e., Banner and Hanson 1990; Jacobsen and Kaufman 1999; Fölling and Frimmel 2002; Halverson et al. 2007; Alvarenga et al. 2014; Kuchenbecker et al. 2016a; Paula-Santos et al. 2017). The $^{87}Sr/^{86}Sr$ ratios range between 0.7074 and 0.7085 display no correlations with the elemental ratios and are considered pristine and to record seawater chemistry. These samples are Sr-rich carbonates, with very low Rb/Sr ratios <0.00014, Fe/Sr ratios <0.1, Mn/Sr ratios <0.05, Mg/Ca ratios <0.018, high Sr contents (Fig. 6), and a high consistency between neighboring samples within each studied section.

Geochemical cross-plot diagrams for the upper 2nd-order sequence display $^{87}Sr/^{86}Sr$ between 0.7074 and 0.7110, showing positive correlations with Rb/Sr, Mn/Sr, Fe/Sr and Mg/Ca ratios (Fig. 6). It indicates post-depositional alteration of the more radiogenic ratios (> 0.7087; Banner and Hanson 1990; Jacobsen and Kaufman 1999; Fölling and Frimmel 2002; Halverson et al. 2007, Alvarenga et al. 2014; Kuchenbecker et al. 2016a; Paula-Santos et al. 2017). Samples with low ratios of $Rb/Sr < 0.0002$, $Mn/Sr < 0.1$, $Fe/Sr < 1.0$ and $Mg/Ca < 0.1$ coupled with Sr contents higher than 700 μg/g exhibit $^{87}Sr/^{86}Sr$ radiogenic ratios between 0.7074 and 0.7085, which are considered records of the primary marine geochemistry during the deposition of the lowermost portion of the upper 2nd-order sequence (Fig. 6).

The regional assessment of post-depositional alteration and diagenesis for each stratigraphic interval demonstrates that fixed values Mn/Sr and Fe/Sr ratios may not be suitable screeners for detecting or deciding between alteration/preservation in carbonates given heterogeneous geochemical signatures that characterize each stage in the basin evolution. Instead flexible ratios and trends are more useful to assess the degree of preservation of carbonates in order to provide a representative Sr isotope chemostratigraphy (Brand et al. 2011; Paula-Santos et al. 2017; Zaky et al. 2019).

5.2. Implications for the marine Sr isotope budget in West Gondwana

Non-radiogenic $^{87}Sr/^{86}Sr$ ratios between 0.7074 and 0.7077 have been interpreted as the representative of the basal Bambuí Group (Misi et al. 2007; Babinski et al. 2007; Kuchenbecker 2011, Kuchenbecker et al., 2016a; Alvarenga et al. 2012, 2014; Caxito et al. 2012, 2018; Paula-Santos et al. 2015). Some authors considered these unradiogenic ratios for global correlation, assigning them to early Ediacaran seawater composition (e.g. Caxito et al. 2012, 2018), while others interpreted them as indicative of restrict marine conditions during the late Ediacaran (Paula-Santos et al. 2017). On the other hand, $^{87}Sr/^{86}Sr$ ratios of 0.7080–0.7084 were initially discarded due to a bias on the post-depositional assessment caused by Sr-enriched carbonates and the lack of basin wide studies to investigate the spatio-temporal significance of these ratios. However, this study attests that primary ratios between 0.7080 and 0.7088 are common in the lower Sete Lagoas Formation (EHST; Fig. 7), succeeding deposition of cap carbonates and preceding the basin wide increase in Sr/Ca ratios. This is in accordance with late Ediacaran fossils and global Sr isotope seawater curves (CI-2 from Paula-Santos et al. 2017). The primary $^{87}Sr/^{86}Sr$ ratios presented here, as well as previous Sr-isotope data reassessed from Arcos section (Kuchenbecker et al. 2016a; Bedoya-Rueda 2019), together with $\delta^{13}C$ values and Sr/Ca ratios, allow a further step in the interpretation of the paleoenvironmental and sedimentary evolution of the Ediacaran-Cambrian Bambuí foreland basin system.

A new feature for the Sr isotope stratigraphy of the Bambuí Group revealed by this study is the relatively rapid fall on the $^{87}Sr/^{86}Sr$ ratios from 0.7086 to 0.7076 through the progradational stage of the lowermost Bambuí 2nd-order sequence (i.e., lower to middle Sete Lagoas Formation) (Fig. 7). This decreasing trend is well observed in Arcos and SMV sections (Figs. 3 and 5). In the Januária section, only two samples showed $^{87}Sr/^{86}Sr$ ratios around 0.7080, and are recorded at the end of the EHST (Fig. 4). This $^{87}Sr/^{86}Sr$ drawdown precedes the $\delta^{13}C$ positive excursion of the basal Bambuí sequence and occurs stratigraphically below than previously suggested by Paula-Santos et al. (2017), which associated this isotope feature with the CI-2/CI-3 boundary (i. e., close to the sequence boundary and associated with the $\delta^{13}C$ positive excursion). This Sr isotope signal can be explained in two hypotheses: 1) stratified water column for $^{87}Sr/^{86}Sr$ ratios and 2) temporal variation of Sr isotopes at basin scale.

The progressive decrease of $^{87}Sr/^{86}Sr$ ratios from 0.7086 to 0.7076 could be a reflect of stratified seawater, according to the facies bathymetry, leading to Sr isotopic gradients with depth (i.e., Shields et al. 1997; Shields 2005; Liu et al. 2014), and the $^{87}Sr/^{86}Sr$ ratios ought to be significantly lower in the shallower environments and higher at greater depths. However, this hypothesis does not seem plausible due to several reasons; a) Sr isotopic heterogeneities produced in stratified oceans have not been well constrained (i.e., Banner 2004); b) stratified seawater models are proposed to explain the formation of cap dolostones in a Snowball Earth context (i.e., Liu et al. 2014); c) are global oceanic models, and d) are short-term duration models (~8 Ky) with rapid carbonate deposition.

The second hypothesis seems to be more consistent, considering the high residence time of Sr (~10^6 years) in the oceans, and the long-term geological history of the Bambuí foreland basin system during several million years at the Ediacaran and Cambrian times (i.e., Kuchenbecker et al. 2020), and therefore, the mechanisms for the progressive fall of $^{87}Sr/^{86}Sr$ ratios in the basal Bambuí Group are better explained by temporal changes of the seawater composition due to paleogeographic chances.

Another implication is that the $^{87}Sr/^{86}Sr$ ratios of ca. 0.7076 seem to match the interval of rare *Cloudina* fossil occurrences in the basin, based on stratigraphic-chemostratigraphic correlations in the Januária city area (in the LHST; Caetano-Filho et al. 2019). This means that late Ediacaran strata in the Bambuí Group present $^{87}Sr/^{86}Sr$ ratios that mismatch the expected ones for coeval open marine basins, if considered global Sr isotope curves (i.e., Halverson et al. 2007; Zaky et al. 2019). Such fall in $^{87}Sr/^{86}Sr$ ratios through EHST to LHST does not seem to be associated with global changes in the oceanic Sr reservoir at the late Ediacaran and early Cambrian, as they are far below than the expected ratios for

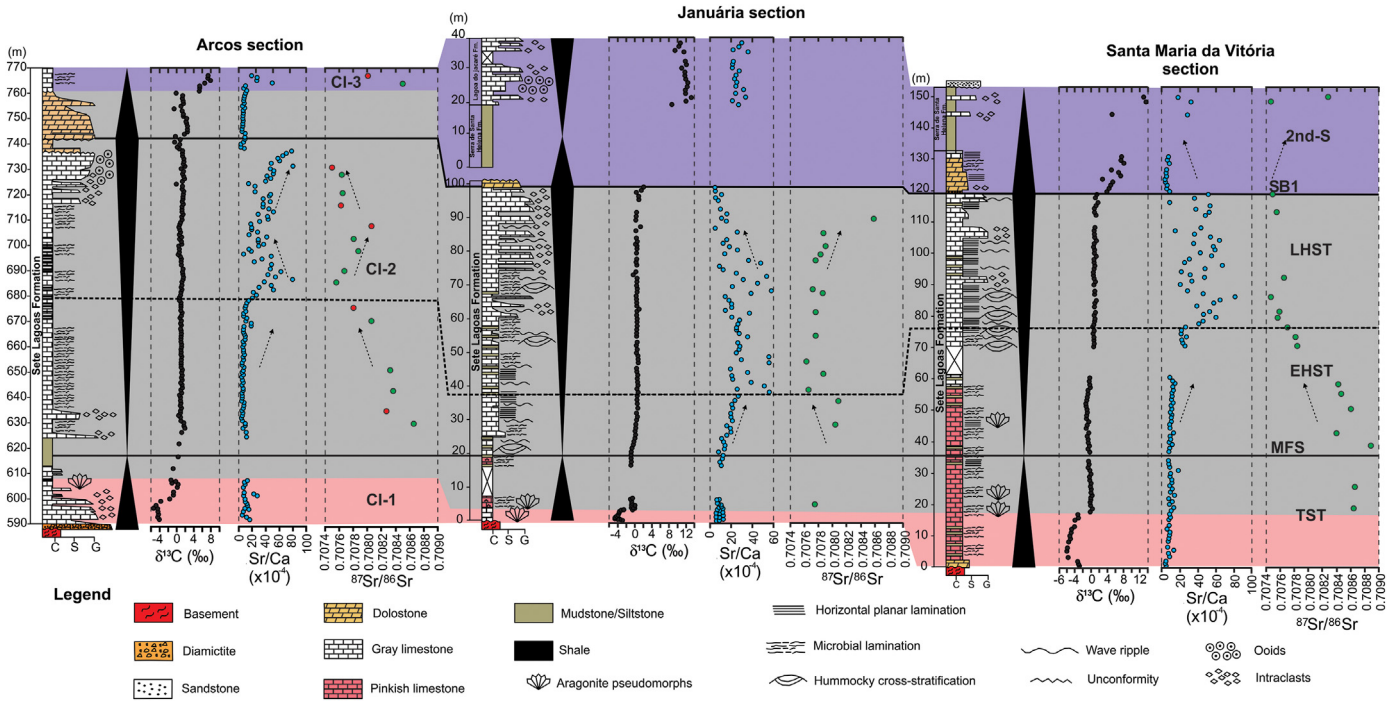

Fig. 7. Stratigraphic-chemostratigraphic correlations for the basal Bambuí Sequence between Arcos, Januária and Santa Maria da Vitória sections. $\delta^{13}C$ and Sr/Ca data presented by Caetano-Filho et al. (2019). TST: Transgressive System Tract; MFS: Maximum Flooding Surface; EHST: Early Highstand System Tract; LHST: Late Highstand System Tract; SB1: Sequence Boundary.

this time period (> 0.7080; i.e., Montañez et al. 1996, 2000; Zaky et al. 2019), and it is associated with other geochemical anomalies, such as basin wide increases in Sr/Ca ratios and succeeded by coupled positive $\delta^{13}C$ excursions reaching superheavy values (Caetano-Filho et al., 2019, 2021). Furthermore, some occurrences of more radiogenic $^{87}Sr/^{86}Sr$ ratios as high as ~0.7085 within Sr-rich interval (LHST of the lowermost 2nd-order sequence and in the overlying 2nd-order sequence; Fig. 7) demonstrates large and sharp $^{87}Sr/^{86}Sr$ variations in the Bambuí sea, which challenge the assumptions based on modern oceanographic Sr system (residence time >> > mixing of ocean waters). Depending on the depositional rates, this sharp transition would represent a rapid geochemical change on seawater, as expected for restricted seas and smaller reservoirs. Therefore, local processes controlling Bambuí Sr isotope chemostratigraphy might have prevailed over global ones.

Similar Sr isotope disturbance is also observed in other late Ediacaran West Gondwana basins bearing *Cloudina* occurrences (i.e., Kawashita 1998; Gaucher et al. 2005; Goméz-Peral et al. 2007). Non-radiogenic $^{87}Sr/^{86}Sr$ ratios are reported in the Rio de la Plata Craton (Arroyo del Soldado Group, Uruguay), with ratios as low as 0.7073 (Gaucher et al. 2005, 2009), and for the Sierras Bayas Group (Argentina), $^{87}Sr/^{86}Sr$ ratios from 0.7070 to 0.7075 (Kawashita 1998, Goméz-Peral et al., 2007), also mismatching the $^{87}Sr/^{86}Sr$ ratios proposed for the Ediacaran and early Cambrian oceans (Paula-Santos et al. 2017). Carbonates deposited in basins formed directly over the basement cratons, such as Rio de la Plata and São Francisco cratons, should record strontium isotope signatures reflecting regional inputs (source areas, aquifers), deviating from the contemporary oceanic water. If the drainage patterns of intracontinental basins were composed of a significant volume of juvenile magmatic rocks or older carbonate rocks, the Sr input on the restricted basins could have had unradiogenic $^{87}Sr/^{86}Sr$ ratios, and thus the calcium carbonate forming in these settings. Therefore, the amalgamation of West Gondwana and related orogenies could have been one of the factors responsible by this regional decrease in Sr ratios recorded in several intracontinental marine basins.

This would not be a singular event in geological time, since other significant temporal $^{87}Sr/^{86}Sr$ variations of seawater have been identified. They were correlated with periods of glaciations, mountain building, major volcanic eruptions or periods of enhanced submarine hydrothermal activity and ocean crust alteration, as well as changes in submarine groundwater discharge and total land area on continents (Peucker-Ehrenbrink and Fiske 2019). These authors argue that the temporal variation in the $^{87}Sr/^{86}Sr$ of seawater is not primarily caused by variations in the balance between radiogenic continental and hydrothermal-related unradiogenic submarine Sr sources. Rather, $^{87}Sr/^{86}Sr$ temporal variations primarily reflect the changing on composition of continental exorheic runoff that is determined by the changing spatial distributions and age of the continental masses, as well as climate and drainage patterns through geological time. In a regional scale, variations in climate and sea-level changes can influence the $^{87}Sr/^{86}Sr$ record of marginal seas such as the Mediterranean, and continental freshwater inputs can locally modify the $^{87}Sr/^{86}Sr$ of coastal waters (i.e., Huang et al. 2011; Beck et al. 2013; Schildgen et al. 2014). In shorter time scales, unradiogenic $^{87}Sr/^{86}Sr$ patterns in Miocene marine basins adjacent to the uplifted Alps and Apennines were attributed to a high influx of Sr from Mesozoic carbonates bearing low $^{87}Sr/^{86}Sr$ exposed in the hinterland, coupled to restricted exchange of water between these basins and the global oceans (Schildgen et al. 2014).

The factors mentioned above could explain the upward decreasing on Sr isotope contents of carbonates from the EHST to the LHST throughout the basin. Changes on the balance between accommodation and carbonate production/sedimentary supply could have changed the spatial distribution of the exorheic continental rivers, increasing geochemical input from dissolved carbonates exposed in catchment areas along the regression, as recorded by the studied highstand systems tract. The increasing tectonic uplift of source areas during the West Gondwana assembly might have also increased the contribution of ancient carbonate rocks to runoff waters (Paula-Santos et al. 2017), as well as the Bambuí carbonate ramp itself recycled by the orogenic activity surrounding the basin. Thus, mountain uplift and chemical weathering of rocks with unradiogenic Sr isotope ratios at regional

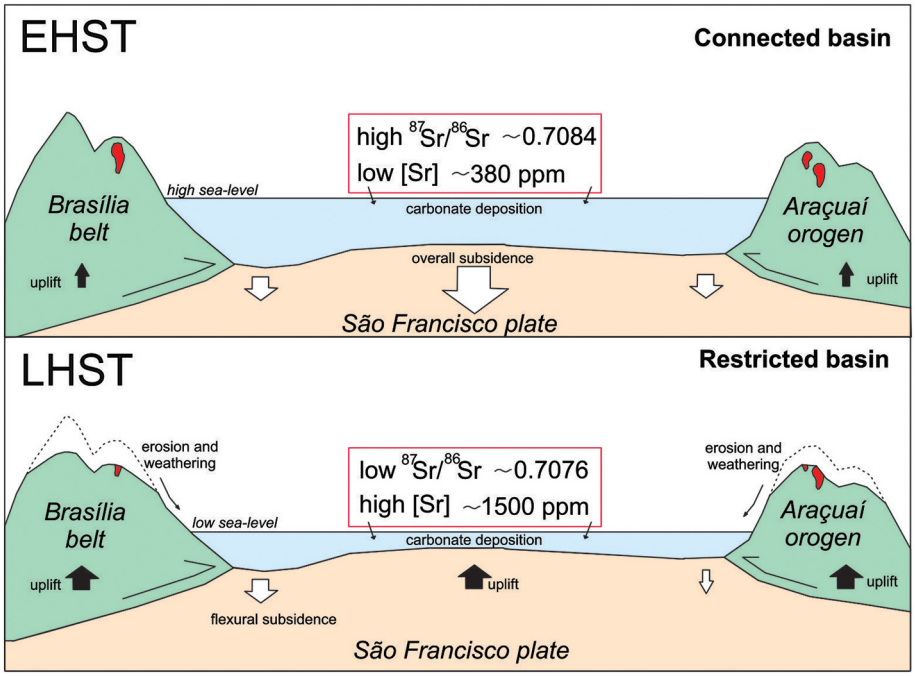

Fig. 8. Sketch illustrating the Bambuí basin and the adjoining orogens at ca. 550 Ma (modified from Kuchenbecker et al. 2020). EHST: connected basin with high relative sea-level associated to overall subsidence; LHST: restricted basin with low relative sea-level associated to flexural subsidence and uplift of marginal orogens.

scale can reasonably explain the homogenization in second order successions and the decrease in the $^{87}Sr/^{86}Sr$ ratios observed from EHST to LHST in the basal Bambuí Group.

Based on this, we suggest that ca. 550 million years ago (i.e., Kuchenbecker et al. 2020), changes on the balance between carbonate production and accommodation associated with tectonically-related flexural subsidence marked by the LHST progressively modified the continental drainage patterns, sedimentary sources and the chemical weathering regimes, altering the strontium influxes and isotopic compositions of the seawater in the early Bambuí basin cycle (Fig. 8). Variations on the contribution from the continents and changes on oceanic water connection due to the drop of the relative sea-level, combined with increased dissolution of ancient hinterland carbonate rocks may be responsible for the drastic decrease in $^{87}Sr/^{86}Sr$ ratios low to ~0.7076 (Fig. 8). This interpretation is supported by coupled basin-wide stratigraphic cycles and geochemical patterns ($^{87}Sr/^{86}Sr$ and Sr/Ca ratios, carbonate REE/PAAS patterns), suggesting these geochemical systems were controlled by the same forcing (e.g., Reis and Suss 2016; Reis et al. 2017; Caetano-Filho et al. 2019; Paula-Santos et al. 2020). It is possible that these mechanisms acted in other coeval West Gondwana basins bearing similar Sr isotope disturbances.

Also, continental inputs into seawater are not restricted to river discharge (Peucker-Ehrenbrink and Fiske 2019). Submarine groundwater discharge (SGD) along the coasts and reactions in estuarine salinity gradients have a potential impact on the marine $^{87}Sr/^{86}Sr$ record (Chaudhuri and Clauer 1986; Basu et al. 2001; Allègre et al. 2010; Beck et al. 2013; Trezzi et al. 2016; Guacaneme et al. 2017; Chakrabarti et al. 2018). This also would have led to great lateral and stratigraphic Sr isotope variability due to regional hydrologic controls on epicontinental seas (McArthur et al. 2001; Doebert et al., 2014; Pietzsch et al. 2018, Peucker-Ehrenbrink and Fiske 2019).

High Sr contents and Sr/Ca ratios, and pristine but variable radiogenic $^{87}Sr/^{86}Sr$ ratios persist through the basal portion of the upper 2nd-order sequence addressed in this work (Fig. 7; except the dolomite-rich intervals). These observations suggest that the Sr budget on the Bambuí seawater was more sensitive to paleoenvironmental changes, probably related to the progressive basin restriction driven by the forelandward advance of the marginal orogenic fronts (Paula-Santos et al. 2017; Uhlein et al. 2019; Caetano-Filho et al. 2019; Kuchenbecker et al. 2020). This is coherent with isotopic and elemental geochemistry that suggest a connected to restricted evolution of the Bambuí foreland basin system, leading to major changes in the seawater patterns, recording an increase in alkalinity, driving fractionation between LREY and HREY, which might have played an important role for biomineralization (Paula-Santos et al. 2020).

The new Sr isotope stratigraphy interpretation proposed here demonstrates that the strontium isotope system recorded the first steps on environmental restriction of the Bambuí foreland basin system, preceding the well-known carbon isotope disturbances to extreme values ($\delta^{13}C_{carb}$ and $\delta^{13}C_{org}$ as high as +16‰ and − 14‰, respectively; Iyer et al. 1995; Caetano-Filho et al., 2021), which have been often associated with the plate reorganizations and environmental changes during the Gondwana assembly (e.g., carbon burial, methanogenesis, increased in $\delta^{13}C$ inputs; Paula-Santos et al. 2017; Uhlein et al. 2019; Caetano-Filho et al., 2021). The high Sr-content and unradiogenic Sr interval observed in the LHST studied here was likely associated with more alkaline and/or hypersaline conditions (Caetano-Filho et al. 2019; Paula-Santos et al. 2020), marking the first tectonically-driven isotope disturbance in the Ediacaran-Cambrian Bambuí basin cycle.

6. Conclusions

Temporal variations of $^{87}Sr/^{86}Sr$ ratios of marine carbonates of the basal Bambuí Group suggest that the Bambuí foreland basin system has evolved from a connected seaway to a restricted sea during the late Ediacaran and early Cambrian, in the context of West Gondwana assembly. A major decrease in the Sr isotope ratios from 0.7086 to 0.7076 is observed coupled to the sequence stratigraphic framework, preceding the positive carbon isotope excursion observed upwards and extending through the middle to upper Bambuí Sequence. Such large variations were not caused by worldwide uniform changes in isotopic compositions of the global Ediacaran-Cambrian seawater reservoir. Instead, these anomalies may have resulted from marine isolation and paleogeographic changes induced by the evolving marginal orogenic systems.

Changes in the chemical weathering regime within surrounding uplifted source areas and variations on the balance between accommodation and carbonate production/sedimentary supply might have been associated with increasingly inputs of unradiogenic $^{87}Sr/^{86}Sr$ by continental waters such as riverine freshwater and groundwater, limited marine dissolution of carbonates, which constitute strong local controls over the Sr isotope compositions of restricted seas. This culminated with a significant change in seawater chemistry and Sr budget and may have contributed to cause large $^{87}Sr/^{86}Sr$ variations coupled to the studied 2nd-order cycles. Similar anomalies in the strontium budget are also recorded in other marine basins of the West Gondwana, suggesting that these mechanisms may have played an important role in continental-scale throughout the late Ediacaran and early Cambrian times.

CRediT authorship contribution statement

Cristian Guacaneme: Data curation, Writing - original draft, Conceptualization, Methodology. **Marly Babinski**: Supervision, Writing - review & editing. **Carolina Bedoya-Rueda**: Visualization, Investigation. **Gustavo M. Paula-Santos**: Conceptualization, Methodology. **Sergio Caetano-Filho**: Conceptualization, Validation. **Matheus Kuchenbecker**: Resources, Writing- Review and Editing. **Humberto L.S. Reis**: Writing-Review and Editing. **Ricardo I.F. Trindade**: Project administration, Funding acquisition.

Declaration of Competing Interest

The authors declare that they have no known competing financial interests or personal relationships that could have appeared to influence the work reported in this paper.

Acknowledgments

This study was funded by the São Paulo Research Foundation (FAPESP) thematic project grant #2016/06114-6, and was also supported by CNPq grant #400764/2016-4. CAPES for the fellowship provided to the first author. Sergio Caetano-Filho holds a FAPESP scholarship grant #2016/11496-5. Gustavo Paula-Santos holds a FAPESP post-doc grant #2017/00399-1. Marly Babinski, Ricardo Trindade and Matheus Kuchenbecker are fellows of the Brazilian Research Council (#307563/2013-8, #206997/2014-0 and #309106/2017-6, respectively). Technical support by Liliane Aparecida Petronilho, which provided the Sr isotope analyses at the CPGeo-USP and Margareth Sugano Navarro for elemental geochemistry at the Laboratory of Isotope Geology-UNICAMP. We would like to thank Jhon Afonso, Kamilla Amorim, Marilia Peloso and Sara dos Santos for field and lab work support and discussions. We are also grateful to Prof. Ian D. Somerville and an anonymous GR reviewer, whose suggestions greatly improved this manuscript.

References

Alkmim, F.F., Martins-Neto, M.A., 2001. A bacia intracratônica do São Francisco: Arcabouço estrutural e cenários evolutivos. In: Pinto, C.P., Martins-Neto, M. (Eds.), A Bacia do São Francisco: geologia e recursos naturais. SBG, Belo Horizonte, pp. 9–30.

Alkmim, F.F., Martins-Neto, M.A., 2012. Proterozoic first-order sedimentary sequences of the São Francisco craton, eastern Brazil. Mar. Pet. Geol. 33, 127–139.

Alkmim, F.F., Marshak, S., Pedrosa-Soares, A.C., Peres, G.G., Cruz, S., Whittington, A., 2006. Kinematic evolution of the Araçuaí-West Congo orogen in Brazil and Africa: nutcracker tectonics during the neoproterozoic assembly of Gondwana. Precambrian Res. 149, 43–64.

Alkmim, F.F., Kuchenbecker, M., Reis, H.L., Pedrosa-Soares, A.C., 2017. The Araçuaí belt. In: Heilbron, M., Cordani, U.G., Alkmim, F.F. (Eds.), Sao Francisco Craton, Eastern Brazil. Tectonic Genealogy of a Miniature Continent. Springer, New York, pp. 255–276.

Allègre, C.J., Louvat, P., Gaillardet, J., Meynadier, L., Rad, S., Capmas, F., 2010. The fundamental role of island arc weathering in the oceanic Sr isotope budget. Earth Planet. Sci. Lett. 292, 51–56. https://doi.org/10.1016/j.epsl.2010.01.019.

Alvarenga, C.J.S., Dardenne, M.A., Vieira, L.C., Martinho, C.T., Guimarães, E.M., Santos, R.V., Santana, R.O., 2012. Estratigrafia da borda ocidental da Bacia do São Francisco. Boletim de Geociências da Petrobras 20, 145–164.

Alvarenga, C.J.S., Santos, R.V., Vieira, L.C., Lima, B.A.F., Mancini, L.H., 2014. Meso-Neoproterozoic isotope stratigraphy on carbonates platforms in the Brasília Belt of Brazil. Precambrian Res. 251, 164–180.

Asmeron, Y., Jacobsen, S.B., Knoll, A.H., Butterfield, N.J., Swett, K., 1991. Strontium isotopic variations of Neoproterozoic seawater: implications for crustal evolution. Geochem. Cosmochim. Acta 55, 2883–2894.

Babinski, M., Vieira, L.C., Trindade, R.I.F., 2007. Direct dating of Sete Lagoas cap carbonate (Bambuí Group, Brazil) and implications for the Neoproterozoic glacial events. Terra Nova 19, 401–406.

Banner, J.L., 2004. Radiogenic isotopes: systematics and applications to earth surface processes and chemical stratigraphy. Earth Sci. Rev. 65, 141–194.

Banner, J.L., Hanson, G.N., 1990. Calculation of simultaneous isotopic and trace element variations during water-rock interaction with application to carbonate diagenesis. Geochim. Cosmochim. Acta 54, 3123–3137.

Basu, A.R., Jacobsen, S.B., Poreda, R.J., Dowling, C.B., Aggarwal, P.K., 2001. Large groundwater strontium flux to the oceans from the Bengal Basin and the marine strontium isotope record. Science 293, 1470–1473. https://doi.org/10.1126/science.1060524.

Beck, A.J., Charette, M.A., Cochran, J.K., Gonneea, M.E., Peucker-Ehrenbrink, B., 2013. Dissolved strontium in the subterranean estuary - Implications for the marine strontium isotope budget. Geochim. Cosmochim. Acta 117, 33–52.

Bedoya-Rueda, C., 2019. Quimiostratigrafia isotópica (C, O, Sr) de alta resolução dos carbonatos da Formação Sete Lagoas, Grupo Bambuí, na região sudoeste da Bacia do São Francisco. Master Thesis. Instituto de Geociências, University of São Paulo, Brazil.

Bellefroid, E.J., Planavsky, N.J., Miller, N.R., Brand, U., Wang, C., 2018. Case study on the utility of sequential carbonate leaching for radiogenic strontium isotope analysis. Chem. Geol. 497, 88–99.

Brand, U., 2004. Carbon, oxygen and strontium isotopes in Paleozoic carbonate components: an evaluation of original seawater–chemistry proxies. Chem. Geol. 204, 23–44. https://doi.org/10.1016/j.chemgeo.2003.10.013.

Brand, U., Veizer, J., 1980. Chemical diagenesis of a multicomponent carbonate system; 1, Trace elements. J. Sediment. Res. 50, 1219–1236. https://doi.org/10.1306/212F7BB7-2B24-11D7-8648000102C1865D.

Brand, U., Veizer, J., 1981. Chemical diagenesis of a multicomponent carbonate system; 2, Stable isotopes. J. Sediment. Res. 51, 987–997. https://doi.org/10.1306/212F7DF6-2B24-11D7-8648000102C1865D.

Brand, U., Logan, A., Bitner, M.A., Griesshaber, E., Azmy, K., Buhl, D., 2011. What is the ideal proxy of Palaeozoic seawater chemistry? Memoirs Assoc. Austr. Palaeontol. 41, 9–24.

Caetano-Filho, S., Paula-Santos, G.M., Guacaneme, C., Babinski, M., Bedoya-Rueda, C., Peloso, M., Amorim, K., Afonso, J., Kuchenbecker, M., Reis, H.L.S., Trindade, R.I.F., 2019. Sequence stratigraphy and chemostratigraphy of an Ediacaran-Cambrian foreland-related carbonate ramp (Bambuí Group, Brazil). Precambrian Res. 331, 105365.

Caetano-Filho, S., Sansjofre, P., Ader, M., Paula-Santos, G.M., Guacaneme, C., Babinski, M., Bedoya-Rueda, C., Kuchenbecker, M., Reis, H., Trindade, R.I.F., 2021. A large epeiric methanogenic Bambuí sea in the core of Gondwana Supercontinent. Geosci. Front. 12, 203–218. https://doi.org/10.1016/j.gsf.2020.04.005.

Campbell, I.H., Squire, R.J., 2010. The mountains that triggered the late Neoproterozoic increase in oxygen: the second great oxidation event. Geochim. Cosmochim. Acta 74 (15), 4187–4206.

Canfield, D.E., Poulton, S.W., Narbonne, G.M., 2007. Late-Neoproterozoic deep-ocean oxygenation and the rise of animal life. Science 315 (5808), 92–95.

Castro, P.T.A., Dardenne, M.A., 2000. The sedimentology, stratigraphy and tectonic context of the São Francisco Supergroup at the southwestern domain of the São Francisco craton, Brazil. Revista Brasileira de Geociências 30, 439–441.

Caxito, F.A., Halverson, G.P., Uhlein, A., Stevensson, R., Dias, T.G., Uhlein, G.J., 2012. Marinoan glaciation in east Central Brazil. Precambrian Res. 200 (203), 38–58.

Caxito, F.A., Uhlein, A., Dantas, E., Stevenson, R., Egydio-Silva, M., Salgado, S.S., 2017. The Rio Preto and Riacho do Pontal Belts. In: Heilbron, M., et al. (Eds.), São Francisco Craton, Eastern Brazil, Regional Geology Reviews https://doi.org/10.1007/978-3-319-01715-0_12.

Caxito, F.A., Frei, R., Uhlein, G.J., Dias, T.G., Árting, T.B., Uhlein, A., 2018. Multiproxy geochemical and isotope stratigraphy records of a neoproterozoic oxygenation event in the Ediacaran Sete Lagoas cap carbonate, Bambuí Group, Brazil. Chem. Geol. 481, 119–132.

Chakrabarti, R., Mondal, S., Shankar, S., Sree, J., Sengupta, D., 2018. Submarine groundwater discharge derived strontium from the Bengal Basin traced in Bay of Bengal water samples. Nature 8, 43–83.

Chaudhuri, S., Clauer, N., 1986. Fluctuations of isotopic composition of strontium in seawater during the Phanerozoic Eon. Chem. Geol. 59, 293–303.

Chiavegatto, J.R.S., Gomes, N.S., Dardenne, M.A., Delgado, C.E.R., 2003. Estratigrafia do Grupo Bambuí nas regiões do norte de Minas Gerais: Uma nova unidade estratigráafic em um contexto de inversão de bacia. SBG, Siimpsio de Geologia de Minas Gerais, Vol. 12. Ouro Preto, Anais, p. 24.

Costa, M.T., Branco, J.R., 1961. Roteiro para a excursão Belo Horizonte-Brasília. Congresso Brasileiro de Geologia 14. UFMG, Inst. Pesq. Radioat., Publ. 15, Belo Horizonte, p. 25.

Dardenne, M.A., 1978. Síntese sobre a estratigrafia do Grupo Bambuí no Brasil Central. Congresso Brasileiro de Geologia, 30, Recife, Anais, SBG, v. 2, pp. 597–610.

DePaolo, D.J., Ingram, B.L., 1985. High-resolution stratigraphy with strontium isotopes. Science 227, 938–942. https://doi.org/10.1126/science.227.4689.938.

Derry, L.A., 2010. A burial diagenesis origin for the Ediacaran Shuram–Wonoka carbon isotope anomaly. Earth Planet. Sci. Lett. 294, 152–162.

Derry, L.A., Kaufman, A.J., Jacobsen, S.B., 1992. Sedimentary cycling and environmental changes in the late Proterozoic: evidence from stable and radiogenic isotopes. Geochim. Cosmochim. Acta 56, 1317–1329.

Doebert, A.C., Johnson, C.M., Carroll, A.R., Beard, B.L., Pietras, J.T., Carson, M.R., Norsted, B., Throckmorton, L.A., 2014. Controls on Sr isotopic evolution in lacustrine systems: Eocene Green River Formation, Wyoming. Chem. Geol. 380, 172–189.

Elderfield, H., 1986. Strontium isotope stratigraphy. Palaeogeogr. Palaeoclimatol. Palaeoecol. 57, 71–90.

Fölling, P.G., Frimmel, H.E., 2002. Chemostratigraphic correlation of carbonate successions in the Gariep and Saldania Belts, Namibia and South Africa. Basin Res. 14, 69–88.

Gaucher, C., Poiré, D.G., Peral, L.G., Chiglino, L., 2005. Litoestratigrafia, bioestratigrafia y correlaciones de las sucesiones sedimentarias Neoproterozoico–Cambrico del Craton del Rio de la Plata (Uruguay y Argentina). Latin Am. J. Sedimentol. Basin Anal. 12 (2), 145–160.

Gaucher, C., Sial, A.N., Poiré, D.G., Gomes-Peral, L., Ferreira, V.P., Pimentel, M.M., 2009. Chemostratigraphy, Neoproterozoic-Cambrian evolution of the Río de la Plata paleocontinent. In: Gaucher, C., Sial, A.N., Halverson, G.P., Frimmel, H.E. (Eds.), Neoproterozoic-Cambrian Tectonics, Global Change and Evolution: A Focus on Southwestern Gondwana Developments in Precambrian Geology. Elsevier, Amsterdam, pp. 115–122.

Goméz-Peral, L.E., Poiré, D.G., Strauss, H., Zimmermann, U., 2007. Chemostratigraphy and diagenetic constraints on Neoproterozoic carbonate successions from the Sierras Bayas Group, Tandilia System, Argentina. Chem. Geol. 237 (1), 109–128.

Guacaneme, C., Babinski, M., Paula-Santos, G.M.D., Pedrosa-Soares, A.C., 2017. C, O, and Sr isotopic variations in Neoproterozoic-Cambrian carbonate rocks from Sete Lagoas Formation (Bambuí Group), in the Southern São Francisco Basin, Brazil. Braz. J. Geol. 47, 521–543.

Halverson, G.P., Dudás, F.O., Maloof, A.C., Bowring, S.A., 2007. Evolution of the $^{87}Sr/^{86}Sr$ composition of Neoproterozoic seawater. Palaeogeogr. Palaeoclimatol. Palaeoecol. 256 (3–4), 103–129.

Halverson, G.P., Wade, B.P., Hurtgen, M.T., Barovich, K.M., 2010. Neoproterozoic chemostratigraphy. Precambrian Res. 182, 337–350.

Heilbron, M., Cordani, U.G., Alkmim, F.F., 2017. The São Francisco Craton and its margins. In: Heilbron, M., et al. (Eds.), São Francisco Craton, Eastern Brazil, Regional Geology Reviews https://doi.org/10.1007/978-3-319-01715-0_1.

Hippertt, J.P., Caxito, F.A., Uhlein, G.J., Nalini, H.A., Sial, A.N., Abreu, A.T., Nogueira, L.B., 2019. The fate of a Neoproterozoic intracratonic marine basin: Trace elements, TOC and IRON speciation geochemistry of the Bambuí Basin, Brazil. Precambrian Res. 330, 101–120.

Hodell, D.A., Mead, G.A., Mueller, P.A., 1990. Variation in the strontium isotopic composition of seawater (8 Ma to present): Implications for chemical weathering rates and dissolved fluxes to the oceans. Chem. Geol. 80, 291–307. https://doi.org/10.1016/0168-9622(90)90011-Z.

Hoffman, P.F., Schrag, D.P., 2002. The Snowball Earth hypothesis: testing the limits of global change. Terra Nova 14, 129–155.

Hoffman, P.F., Kaufman, A.J., Halverson, G.P., Schrag, D.P., 1998. A Neoproterozoic Snowball Earth. Science 281, 1342–1346.

Huang, K.-F., You, C.-F., Chung, C.-H., Lin, I.-T., 2011. Nonhomogeneous seawater Sr isotopic composition in the coastal oceans: a novel tool for tracing water masses and submarine groundwater discharge. Geochem. Geophys. Geosyst. 12 (5), Q05002. https://doi.org/10.1029/2010GC003372.

Ingram, B.L., Sloan, D., 1992. Strontium isotopic composition of estuarine sediments as paleosalinity-paleoclimate indicator. Science 255, 68–72.

Iyer, S.S., Babinski, M., Krouse, H.L., Chemale, F., 1995. Highly ^{13}C-enriched carbonate and organic matter in the Neoproterozoic sediments of the Bambuí Group, Brazil. Precambrian Res. 73, 271–282.

Jacobsen, S.B., Kaufman, A.J., 1999. The Sr, C and O isotopic evolution of Neoproterozoic seawater. Chem. Geol. 161, 37–57.

Kaufman, A.J., Jacobsen, S.B, Knoll, A.H., 1993. The Vendian record of Sr and C-isotopic variations in seawater - implications for tectonics and paleoclimate. Earth and Planetary Science Letters 120, 409–430.

Kaufman, A.J., Knoll, A.H., 1995. Neoproterozoic variations in the C-isotopic composition of seawater: stratigraphic and biogeochemical implications. Precambr. Res. 73, 27–49. https://doi.org/10.1016/0301-9268(94)00070-8.

Kawashita, K., 1998. Rochas carbonáticas neoproterozoicas da América do Sul: idades e inferências quimioestratigráficas. Livre Docência Thesis. University of São Paulo, Brazil.

Knoll, A.H., Walter, M.R., Narbonne, G.M., Christie-Blick, N., 2006. The Ediacaran Period: a new addition to the geologic time scale. Lethaia 39, 13–30.

Krabbenhoft, A., Eisenhauer, A., Bohm, F., Vollstaedt, H., Fietzke, J., Liebetrau, V., 2010. Constraining the marine strontium budget with natural strontium isotope fractionations ($^{87}Sr/^{86}Sr$, $\delta^{88}/^{86}Sr$) of carbonates, hydrothermal solutions and river waters. Geochim. Cosmochim. Acta 74, 4097–4109.

Kuchenbecker, M., 2011. Quimioestratigrafia e proveniência sedimentar da porção basal do Grupo Bambuí em Arcos (MG). Master Thesis. Universidade Federal de Minas Gerais, Belo Horizonte, p. 91.

Kuchenbecker, M., Babinski, M., Pedrosa-Soares, A.C., Costa, R.D., Lopes-Silva, L., Pimenta, F., 2013. Proveniência e análise sedimentar da porção basal do Grupo Bambuí em Arcos (MG). Geologia USP 13 (4), 49–61.

Kuchenbecker, M., Babinski, M., Pedrosa-Soares, A.C., Lopes-Silva, L., Pimenta, F., 2016a. Chemostratigraphy of the lower Bambuí Group, southwestern São Francisco Craton, Brazil: insights on Gondwana paleoenvironments. Braz. J. Geol. 46, 145–162.

Kuchenbecker, M., Atman, D., Costa, R.D., Pedrosa-Soares, A.C., Babinski, M., 2016b. A formação Gorutuba: sedimentação litorânea a continental na margem leste da Bacia Bambuí (MG). Geologia USP Série Científica 16 (2), 67–81.

Kuchenbecker, M., Pedrosa-Soares, A.C., Babinski, M., Reis, H.L.S., Atman, D., Costa, R.D., 2020. Towards an integrated tectonic model for the interaction between the Bambuí basin and the adjoining orogenic belts: evidences from the detrital zircon record of syn-orogenic units. J. S. Am. Earth Sci. 104, 102831.

Kuznetsov, A.B., Gorokhov, I.M., Semikhatov, M.A., Mel'nikov, N.N., Kozlov, V.I., 1997. Strontium isotopic composition in the limestones of the Inzer Formation, Upper Riphean type section, southern Urals. Trans. Russian Acad. Sci. Earth Sci. Sect. 353, 319–324.

Kuznetsov, A.B., Ovchinnikova, G.V., Gorokhov, I.M., Letnikova, E.F., Kaurova, O.K., Konstantinova, G.V., 2013. Age constraints on the Neoproterozoic Baikal Group from combined Sr isotopes and Pb-Pb dating of carbonates from the Baikal type section, southeastern Siberia. J. Asian Earth Sci. 62, 51–66.

Li, D., Shields-Zhou, G.A., Ling, H.-F., Thirlwall, M., 2011. Dissolution methods for strontium isotope stratigraphy: guidelines for the use of bulk carbonate and phosphorite rocks. Chem. Geol. 290, 133–144. https://doi.org/10.1016/j.chemgeo.2011.09.004.

Liu, C., Wang, Z., Raub, T.D., Macdonald, F.A., Evans, D.A.D., 2014. Neoproterozoic cap-dolostone deposition in stratified glacial meltwater plume. Earth Planet. Sci. Lett. 404, 22–32.

Martins, M., Lemos, V.B., 2007. Análise estratigráfica das sequências neoproterozoicas da Bacia do São Francisco. Revista Brasileira de Geociências 37 (4), 156–167.

Martins-Neto, M.A., 2005. A Bacia do São Francisco: arcabouços estratigráfico e estrutural com base na integração de dados de superfície e subsuperfície. Simpósio sobre o Cráton do São Francisco, III, Salvador/BA, 2005, Anais, pp. 283–286.

Martins-Neto, M.A., 2009. Sequence stratigraphic framework of Proterozoic successions in eastern Brazil. Mar. Pet. Geol. 26, 163–176.

McArthur, J.M., Howarth, R.J., Bailey, T.R., 2001. Strontium isotope stratigraphy: LOWESS version 3: best fit to the marine Sr-isotope curve for 0–509 Ma and accompanying look-up table for deriving numerical age. J. Geol. 109, 155–170. https://doi.org/10.1086/319243.

McArthur, J.M., Howarth, R.J., Shields, G.A., 2012. Chapter 7 – Strontium isotope stratigraphy. The Geologic Time Scale 1, 127–144. https://doi.org/10.1016/B978-0-444-59425-9.00007-X.

Melezhik, V.A., Gorokhov, I.M., Kuznetsov, A.B., Fallick, A.E., 2001. Chemostratigraphy of Neoproterozoic carbonates: implications for "blind dating". Terra Nova 13, 1–11.

Misi, A., Kaufman, A.J., Veizer, J., Powis, K., Azmy, K., Boggiani, P.C., Gaucher, C., Teixeira, J.B.G., Sanchez, A.L., Iyer, S.S.S., 2007. Chemostratigraphic correlation of Neoproterozoic successions in South America. Chem. Geol. 237, 143–167.

Montañez, I.P., Banner, J., Osleger, D.A., Borg, L.E., Bosserman, P.J., 1996. Integrated Sr isotope variations and sea-level history of Middle to Upper Cambrian platform carbonates: Implications for the evolution of Cambrian seawater $^{87}Sr/^{86}Sr$. Geology 24-10, 917–920.

Montañez, I.P., Osleger, D.A., Banner, J.L., Mack, L.E., Musgrove, M., 2000. Evolution of the Sr and C Isotope Composition of Cambrian Oceans. GSA Today 10–15.

Moreira, D.S., Uhlein, A., Dussin, I.A., Uhlein, G.J., Misuzaki, A.M., 2020. A Cambrian age for the upper Bambuí Group, Brazil, supported by the first U-Pb dating of volcaniclastic bed. J. S. Am. Earth Sci. https://doi.org/10.1016/j.jsames.2020.102503.

Palmer, M.R., Edmond, J.M., 1989. The strontium isotope budget of the modem ocean. Earth Planet. Sci. Lett. 92, 11–26.

Paula-Santos, G.M., Babinski, M., Kuchenbecker, M., Caetano-Filho, S., Trindade, R.I., Pedrosa-Soares, A.C., 2015. New evidence of an Ediacaran age for the Bambuí Group in southern São Francisco craton (eastern Brazil) from zircon U-Pb data and isotope chemostratigraphy. Gondwana Res. 28, 702–720.

Paula-Santos, G.M., Caetano-Filho, S., Babinski, M., Trindade, R.I., Guacaneme, C., 2017. Tracking connection and restriction of West Gondwana São Francisco Basin through isotope chemostratigraphy. Gondwana Res. 42, 280–305.

Paula-Santos, G.M., Caetano-Filho, S., Babinski, M., Enzweiler, J., 2018. Rare earth elements of carbonate rocks from the Bambuí Group, southern São Francisco Basin, Brazil, and their significance as paleoenvironmental proxies. Precambrian Res. 305, 327–340.

Paula-Santos, G.M., Caetano-Filho, S., Enzweiler, J., Navarro, M.S., Babinski, M., Guacaneme, C., Kuchenbecker, M., Reis, H., Trindade, R.I.F., 2020. Rare earth elements in the terminal Ediacaran Bambuí Group carbonate rocks (Brazil): evidence for high seawater alkalinity during rise of early animals. Precambrian Res. 336, 105506.

Perrella, P., Uhlein, A., Uhlein, G.J., Sial, A.N., Pedrosa-Soares, A.C., Lima, O.N.B., 2017. Facies analysis, sequence stratigraphy and chemostratigraphy of the Sete Lagoas Formation (Bambuí Group), northern Minas Gerais State, Brazil: evidence of a cap carbonate deposited on the Januária basement high. Braz. J. Geol. 47, 59–77.

Peucker-Ehrenbrink, B., Fiske, G.J., 2019. A continental perspective of the seawater $^{87}Sr/^{86}Sr$ record: a review. Chem. Geol. 510, 140–165.

Pietzsch, R., Oliveira, D.M., Tedeschi, L.R., Queiroz Neto, J.V., Figueiredo, M.F., Vazquez, J.C., Souza, R.S., 2018. Palaeohydrology of the lower cretaceous pre-salt lacustrine system, from rift to post-rift phase, Santos Basin, Brazil. Palaeogeogr. Palaeoclimatol. Palaeoecol. 507, 60–80.

Pimentel, M.M., Fuck, R.A., Botelho, N.F., 1999. Granites and the geodynamic history of the Neoproterozoic Brasilia belt, Central Brazil: a review. Lithos 46 (3), 463–483.

Reis, H.L.S., Suss, J.F., 2016. Mixed carbonate-siliciclastic sedimentation in forebulge grabens: an example from the Ediacaran Bambuí Group, São Francisco basin, Brazil. Sediment. Geol. 339, 83–103.

Reis, H.L.S., Alkmim, F.F., Fonseca, R.C.S., Nascimento, T.C., Suss, J.F., Prevatti, L.D., 2016. The São Francisco Basin. In: Heilbron, M., Cordani, U.G., Alkmim, F.F. (Eds.), São Francisco Craton, Eastern Brazil, Regional Geology Reviews. Springer, Switzerland, pp. 117–143.

Reis, H.L.S., Suss, J.F., Fonseca, R.C.S., Alkmim, F.F., 2017. Ediacaran forebulge grabens of the southern São Francisco basin, SE Brazil: Craton interior dynamics during West Gondwana assembly. Precambrian Res. 302, 150–170.

Santos, R.V., Alvarenga, C.J.S., Dardenne, M.A., Sial, A.N., Ferreira, V.P., 2000. Carbon and oxygen isotope profiles across Meso-Neoproterozoic limestones from Central Brazil: Bambuí and Paranoá groups. Precambrian Res. 104, 107–122.

Santos, R.V., Alvarenga, C.J.S., Babinski, M., Ramos, M.L.S., Cukrov, N., Fonseca, M.A., Sial, A.N., Dardenne, M.A., Noce, C.M., 2004. Carbon isotopes of Mesoproterozoic–Neoproterozoic sequences from Southern São Francisco craton and Araçuaí Belt, Brazil: Paleogeographic implications. J. S. Am. Earth Sci. 18, 27–39.

Schildgen, T.F., Cosentino, D., Frijia, G., Castorina, F., Dudas, O., Iadanza, A., Sampalmieri, G., Cipollari, P., Caruso, A., Bowring, S.A., Strecker, M.R., 2014. Sea level and climate forcing of the Sr isotope composition of late Miocene Mediterranean marine basins. Geochem. Geophys. Geosyst. 15, 2964–2983. https://doi.org/10.1002/2014GC005332.

Shields, G.A., 2005. Neoproterozoic cap carbonates: a critical appraisal of existing models and the plumeworld hypothesis. Terra Nova 17 (4), 299–310.

Shields, G.A., Stille, P., Brasier, M.D., Atudorei, N., 1997. Stratified oceans and oxygenation of the late Precambrian environment: a post glacial geochemical record from the Neoproterozoic of W. Mongolia. Terra Nova 9, 218–222.

Trezzi, G., Garcia-Orellana, J., Rodellas, V., Masque, P., Garcia-Solsona, E., Andersson, P.S., 2016. Assessing the role of submarine groundwater discharge as a source of Sr to the Mediterranean Sea. Geochim. Cosmochim. Acta, GCA10057 https://doi.org/10.1016/j.gca.2016.12.005.

Uhlein, A., Baptista, M.C., Seer, H.J., Caxito, F.A., Uhlein, G.J., Dardenne, M.A., 2011. A Formação Lagoa Formosa, Grupo Bambuí (MG): Sistema deposicional de leque submarino em bacia de antepaís. Geonomos 19 (2), 163–172.

Uhlein, G.J., Uhlein, A., Stevenson, R., Halverson, G.P., Caxito, F.A., Cox, G.M., 2017. Early to late Ediacaran conglomeratic wedges from a complete foreland basin cycle in the Southwest São Francisco Craton, Bambuí Group, Brazil. Precambrian Res. 299, 101–116.

Uhlein, G.J., Uhlein, A., Pereira, E., Caxito, F.A., Okubo, J., Warren, L.V., Sial, A.N., 2019. Ediacaran paleoenvironmental changes recorded in the mixed carbonate siliciclastic Bambuí Basin, Brazil. Palaeogeogr. Palaeoclimatol. Palaeoecol. 517, 39–51.

Valeriano, C.M., 2017. The southern Brasília belt. In: Heilbron, M., Cordani, U.G., Alkmim, F.F. (Eds.), São Francisco Craton, Eastern Brazil: Tectonic Genealogy of a Miniature Continent. Springer International Publishing, Switzerland, pp. 189–204.

Veizer, J., Compston, W., Clauer, N., Schidlowski, M., 1983. $^{87}Sr/^{86}Sr$ in late Proterozoic carbonates: evidence for a mantle event at 900 Ma ago. Geochim. Cosmochim. Acta 47, 295–302.

Veizer, J., Hoefs, J., Ridler, R.H., Jensen, L.S., Lowe, D.R., 1989. Geochemistry of Precambrian carbonates: I. Archean hydrothermal systems. Geochim. Cosmochim. Acta 53, 845–857.

Veizer, J., Ala, D., Azmy, K., Brukschen, P., Buhl, D., Bruhn, F., Carden, G.A.F., Diener, A., Ebneth, S., Godderis, Y., Jasper, T., Korte, C., Pawellek, F., Podlaha, O.G., Strauss, H., 1999. $^{87}Sr/^{86}Sr$, $\delta^{13}C$ and $\delta^{18}O$ evolution of Phanerozoic seawater. Chem. Geol. 161, 59–88.

Vieira, L.C., Almeida, R.P., Trindade, R.I.F., Nogueira, A.C.R., Janikian, L., 2007a. Formação Sete Lagoas em sua área-tipo: fácies, estratigrafia e sistemas deposicionais. Revista Brasileira de Geociências 37, 1–4.

Vieira, L.C., Nédélec, A., Fabre, S., Trindade, R.I.F., Almeida, R.P., 2015. Aragonite crystal fans in Neoproterozoic cap carbonates: a case study from Brazil and implications for the post-snowball earth coastal environment. Journal of Sedimentary Research 85, 285–300. https://doi.org/10.2110/jsr.2015.21.

Vieira, L.C., Trindade, R.I.F., Nogueira, A.C.R., Ader, M., 2007b. Identification of a Sturtian cap carbonate in the Neoproterozoic Sete Lagoas carbonate plataform, Bambuí Group, Brazil. Compt. Rendus Geosci. 339, 240–258.

Warren, L.V., Quaglio, F., Riccomini, C., Simões, M.G., Poiré, D.G., Strikis, N.M., Anelli, L.E., Strikis, P.C., 2014. The puzzle assembled: Ediacaran guide fossil Cloudina reveals an old proto-Gondwana seaway. Geology 42 (5), 391–394.

Wei, G., Hood, A.V.S., Chen, Xi, Li, D., Wei, W., Wen, B., Gong, Z., Yang, T., Zhang, Z., Ling, H., 2019. Ca and Sr isotope constraints on the formation of the Marinoan cap dolostones. Earth Planet. Sci. Lett. 511, 202–212.

Young, G.M., 2013. Evolution of Earth's climatic system: Evidence from ice ages, isotopes, and impacts. GSA Today 23, 10.

Zaky, A.M., Brand, U., Buhl, D., Blamey, N.M., Bitner, A., Logan, A., Gaspard, D., Popov, A., 2019. Strontium isotope geochemistry of modern and ancient archives: tracer of secular change in ocean chemistry. Can. J. Earth Sci. 56, 245–264.